



Planetary Albedo Change Exacerbates Surface Warming: A Perspective From Cloud Transition

Ruixue Li¹, Jiming Li¹, Bida Jian¹, Lijie Zhang¹, Jiayi Li¹

¹Key Laboratory for Semi-Arid Climate Change of the Ministry of Education, College of Atmospheric Sciences, Lanzhou University, Lanzhou, China

5

Corresponding author: Jiming Li (lijiming@lzu.edu.cn)

Abstract. Persistent global warming is modulated by cloud changes, yet the specific contributions and mechanisms remain inadequately quantified. Using CERES radiation data with a surface energy-balance framework, we quantify the contribution of cloud radiative changes to decadal surface temperature trends over 2002–2023. Cloud changes exert a weak net effect on global mean warming due to near-cancellation between shortwave warming and longwave cooling, but strongly modulate its spatial pattern. Specifically, clouds enhance warming in low- and mid-latitudes while mitigating warming at high latitudes. This pattern is driven by systematic transitions from low-/mid- to high-level optically thin clouds, which reduce planetary albedo and weaken cloud longwave emission. These changes exhibit hemispheric difference. In 30–60°N, the region contributing most to global warming, the decline in the cloud-reflected solar radiation is mainly driven by decreased cloud fraction, linked to elevated sea surface temperatures, aerosol reductions, and mid-tropospheric drying. In 30–60°S, reduced cloud reflectivity resulting from decreased cloud optical thickness and increased liquid droplet radius dominates, partly offset by shifts from cumulus to stratocumulus. However, at high latitudes in both hemispheres, increased mid-/high-clouds and enhanced cloud reflectivity, driven by enhanced moisture, upper-tropospheric static stability and increased cloud optical thickness, lead to greater reflected solar radiation and reduced downwelling longwave radiation, thereby attenuating local warming. Our results establish a direct observational link between cloud transitions, planetary albedo decline, and spatially heterogeneous warming, providing a constraint on cloud feedbacks in recent climate change.

30



1 Introduction

Over the past two decades, the Earth is experiencing unprecedented warming, which exacerbates global heatwaves, wildfires, droughts, and glacier melt, while also
35 poses increasing threats to human health and life (Ripple et al., 2024; Gould et al., 2025). The 2023–2024 period experienced frequent record-breaking global mean surface temperatures (Li et al., 2024a; Cheng et al., 2025). While such record-breaking temperatures may be influenced by internal variability (Goessling et al., 2024; Li et al., 2024a; Blanchard-Wrigglesworth et al., 2025; Minobe et al., 2025), such as the El Niño–
40 Southern Oscillation (ENSO), the magnitude of these extremes would be improbable without an underlying and sustained warming trend driven by earth’s energy accumulation. This urges us to identify the underlying reasons behind the persistent global warming.

While the role of longwave radiation changes driven by factors such as greenhouse
45 gases and aerosols in surface warming has been extensively studied, the contribution of shortwave radiation has often been overlooked. Planetary albedo (PA), which regulates the absorption and distribution of solar energy, plays a critical role in controlling surface temperature (T_s). A record-low PA has been identified as a key driver of both recent extreme temperature anomalies (Goessling et al., 2024) and marine heatwaves (Dong
50 et al., 2025), while its accurate representation has proven crucial for improving the predictive skill of climate models (Blanchard-Wrigglesworth et al., 2025). Clouds, as the dominant regulator of PA (Stephens et al., 2015; Jian et al., 2018; Loeb et al., 2021; Li et al., 2024b; Li et al., 2025), influence the amount of solar radiation reaching the surface and thereby affect T_s . Liu et al. (2024) have highlighted that, after accounting
55 for near-surface air temperature feedbacks, cloud radiative effects are the primary physical process driving monthly T_s variability over land. Under global warming, it means that changes in dynamical and meteorological conditions may trigger adjustments in cloud type, coverage, and albedo (i.e., cloud transitions), thereby altering cloud radiative properties. Several model simulations have emphasized changes in
60 cloud feedbacks under global warming. For example, Ceppi and Hartmann (2016) demonstrated that shortwave cloud radiative changes substantially intensify meridional temperature gradients and dominate the poleward expansion of large-scale circulation systems. Similarly, Zelinka et al. (2020) found that enhanced positive low-cloud feedbacks in CMIP6 models, driven by decreased extratropical low-cloud amount and



65 optical depth, are the primary cause of their higher effective climate sensitivity. In
addition, observations also reveal the extensive changes in cloud properties in recent
years. Several studies have reported the reductions in low cloud cover at low-mid
latitudes (Goessling et al., 2024; Loeb et al., 2024; Minobe et al., 2025). From a
macroscopic perspective, Tselioudis et al. (2025) indicated that the contraction of storm
70 zones drives the observed increase in global solar absorption. However, the contribution
of these cloud changes to long-term T_s trends remains unquantified, and there is no
observational evidence to support which specific cloud property changes have been
most responsible.

To address these gaps, this study quantitatively assesses the radiative contribution
75 of clouds to decadal T_s trends over 2002–2023 using satellite radiation data within a
surface energy-balance framework. By isolating the cloud component of PA and
decomposing it into cloud fraction and intrinsic cloud reflectivity for different cloud
regimes, we separate their respective roles and further identify the underlying
mechanisms. This observation-based attribution provides a robust benchmark for
80 evaluating the representation of cloud radiative effects in climate models and offers new
insights into the cloud feedback processes that influence recent warming trends.

2 Data and Methodology

2.1 CERES data

This study uses radiation and cloud data from July 2002 to February 2023 obtained
85 from the Clouds and the Earth's Radiant Energy System (CERES) project. Two primary
CERES products are employed: the Energy Balanced and Filled (EBAF) Edition 4.2.1
to quantify cloud radiative impacts on T_s trends and decompose PA, and the
FluxbyCldTyp (FBCT) Edition 4.1 to analyze cloud-type changes.

We use monthly mean observed incoming solar radiation (ISR) and reflected
90 shortwave radiation (RSR) at the top of atmosphere (TOA), alongside computed surface
upwelling and downwelling shortwave and longwave radiation fluxes at 1° resolution
from EBAF (Wielicki et al., 1996; Kato et al., 2018; Loeb et al., 2018). This product
provides diurnally complete averages by integrating geostationary satellite corrections
(Loeb et al., 2018). Moreover, it ensures temporal continuity across satellite transitions
95 and applies objective constraint algorithm to achieve energy balance closure based on
ocean heat storage estimates (Loeb et al., 2009).



The FBCT Terra+Aqua Edition 4.1 product provides cloud-type partitioned radiative fluxes and cloud properties across pressure and optical depth bins (Sun et al., 2022), derived from CERES Single Scanner Footprint (SSF) Edition 4A and Moderate Resolution Imaging Spectroradiometer (MODIS) data. Both single-layer and multi-layer portions of upper-level clouds are classified as upper-level clouds. In this study, we employ 1° gridded monthly mean regional clear-sky shortwave fluxes, along with shortwave fluxes, cloud fraction (CF), cloud visible optical depth (CVOD), liquid cloud particle radius (r_{liq}) and ice cloud particle radius (r_{ice}) for different cloud types. Following the cloud type classification from International Satellite Cloud Climatology Project (ISCCP), we classify the clouds into nine types based on cloud top pressure and optical depth: cumulus (Cu), stratocumulus (Sc), stratus (St), altocumulus (Ac), altostratus (As), nimbostratus (Ns), cirrus (Ci), cirrostratus (Cs), cumulonimbus (Cb).

The shortwave cloud radiative forcing at the TOA ($SWCRF_{TOA}$) for the specific cloud type c is defined as:

$$SWCRF_{TOA,c} = CF_c \times (RSR_c - RSR_{clr}) \quad (1)$$

where RSR_c is the upwelling overcast TOA flux for that cloud type, RSR_{clr} is the upwelling clear-sky TOA flux, and CF_c is the cloud fraction of that type. The term in parentheses represents the change in reflected shortwave radiation per unit cloud cover—i.e., the intrinsic shortwave cloud radiative effect of the cloud itself. We refer to this quantity as cloud reflectivity (CR):

$$CR_c = RSR_c - RSR_{clr} \quad (2)$$

CR is determined by the cloud's own microphysical properties, such as cloud thickness and the size of water droplets or ice crystals within the cloud. Multiplying CR by the corresponding cloud fraction yields the total shortwave cloud radiative forcing contributed by that cloud type.

The variable, $SWCRF_{TOA,c}$, is only used in decomposing the cloud component of RSR in Section 2.4. The classification thresholds and global mean climatology of CF and CR are provided in Fig. S1.

2.2 Reanalysis data

In this study, monthly skin temperature data are obtained from the ECMWF Reanalysis v5 (ERA5). To further investigate the thermodynamic and dynamic drivers of cloud changes, several key monthly averaged meteorological variables from ERA5



are employed. Additionally, the aerosol optical depth (AOD) data from MERRA-2 are
130 used to assess the potential influence of aerosols on cloud microphysics (Kaufman et
al., 2005). The specific cloud controlling factors used are detailed in Section 2.5 and
Table 1. All reanalysis datasets are regridded to a $1^\circ \times 1^\circ$ spatial resolution to match with
the CERES data.

2.3 Radiative Contribution of Clouds to Surface Warming

135 Radiative forcing and climate feedbacks are often diagnosed using radiation fluxes
at the TOA, which provide a useful framework for understanding global energy balance
and temperature responses (Bony et al., 2006). However, regional T_s changes are
strongly influenced by atmospheric and oceanic energy transports, so local temperature
variations are not necessarily directly tied to TOA radiative anomalies (Liu et al., 2024).
140 Therefore, examining the surface energy budget provides a more direct way to relate T_s
changes to local radiative and turbulent energy fluxes (Andrews et al., 2009; Lu and
Cai, 2009; Colman, 2015; Boeke and Taylor, 2018; Sejas et al., 2021), motivating the
surface energy balance framework used in this study.

Following Lu and Cai (2009), we can quantify the contribution of clouds to T_s
145 changes through both shortwave and longwave pathways. The monthly anomaly of T_s
for each grid can be decomposed into contributions from different physical processes
based on the surface energy balance equation (Lu and Cai, 2009):

$$\Delta T_s \approx \{ -(\Delta\alpha)(\overline{SW^\downarrow} + \Delta SW^\downarrow) + \Delta CRF_S + (1 - \bar{\alpha})\Delta SW_{clr}^\downarrow + \Delta LW_{clr}^\downarrow - \Delta Q - \Delta(SH + LE) \} / 4\sigma\bar{T}_s^3 \quad (3)$$

Each term on the right-hand side represents the contribution to T_s anomalies from
150 distinct physical processes:

(a) Surface albedo feedback (SAF): $-(\Delta\alpha)(\overline{SW^\downarrow} + \Delta SW^\downarrow)$

(b) Surface cloud radiative forcing:

$$\Delta CRF_S = (1 - \bar{\alpha})\Delta SW_{clr}^\downarrow + \Delta LW_{clr}^\downarrow \quad (4)$$

(c) Non-SAF-induced clear-sky shortwave radiation: $(1 - \bar{\alpha})\Delta SW_{clr}^\downarrow$

155 (d) Clear-sky downward longwave radiation: $\Delta LW_{clr}^\downarrow$

(e) Surface heat storage (includes oceanic energy transport in oceans): $-\Delta Q$

(f) Combined sensible and latent heat fluxes: $-\Delta(SH + LE)$

Here, Δ denotes monthly anomalies relative to the climatological mean; overbars
indicate monthly climatological means; α is surface albedo; SW (LW) denotes



160 shortwave (longwave) radiation flux; downward arrows represent surface downward
fluxes; SH (LE) represents sensible (latent) heat flux; and σ is the Stefan-Boltzmann
constant. Subscripts clr and cld refer to clear-sky and cloudy conditions, respectively,
with cloudy conditions calculated as the difference between all-sky and clear-sky
conditions. Temperature units are in Kelvin (K).

165 Therefore, the monthly T_s anomalies caused by changes in surface cloud radiative
forcing (ΔCRC , units: K) at each grid point is calculated as:

$$\Delta CRC = \{(1 - \bar{\alpha})\Delta SW_{cld}^{\downarrow} + \Delta LW_{cld}^{\downarrow}\} / 4\sigma \bar{T}_s^3 \quad (5)$$

The ΔCRC comprehensively captures both the shortwave radiative influences of
clouds on T_s (ΔCRC_{sw}), which is not induced by surface albedo feedback, and the
170 longwave radiative influences of clouds on T_s (ΔCRC_{lw}).

$$\Delta CRC_{sw} = (1 - \bar{\alpha})\Delta SW_{cld}^{\downarrow} / 4\sigma \bar{T}_s^3 \quad (6)$$

$$\Delta CRC_{lw} = \Delta LW_{cld}^{\downarrow} / 4\sigma \bar{T}_s^3 \quad (7)$$

To analyze latitudinal patterns, we calculate area-weighted regional averages of
 ΔCRC within 30° latitude zones. The resulting time series for each latitudinal zone are
175 then used to determine trends, representing the T_s trends caused by cloud radiative
changes across different latitude zones (CRC_{sw} and CRC_{lw}).

The surface energy balance decomposition provides a useful diagnostic framework
for quantifying the contributions of different energy flux components to T_s anomalies.
However, its application over oceanic regions warrants careful interpretation. Over
180 oceans, the large heat capacity of the ocean mixed layer and the influence of horizontal
heat transport can result in a non-negligible local surface energy imbalance term
(Donohoe & Battisti, 2013; Sejas et al., 2021). In addition, turbulent heat fluxes and
ocean heat storage may covary with cloud radiative forcing. For instance, Liu et al.
(2024) showed that over land, the cloud radiative effect is largely offset by its negative
185 covariance with turbulent heat fluxes, as reduced cloud cover enhances surface heat
loss. Therefore, the quantity ΔCRC derived from Eq. (5) should be interpreted as the
direct radiative contribution associated with cloud changes under the linearized surface
energy balance framework, rather than a complete attribution of T_s variability. Despite
this limitation, the approach has been employed to diagnose the radiative effects of
190 clouds on T_s at global scales, including over oceans (Izumi et al., 2014).

2.4 Decomposition of the cloud component of TOA RSR



In order to further clarify how clouds modulate solar radiation reaching the Earth's surface, we isolate the cloud component of TOA RSR, denoted as RSR_{cloud} , which represent the direct radiative effect of clouds on the TOA reflected shortwave radiation.

195 Following the simplified radiative model (Donohoe and Battisti, 2011; Stephens et al., 2015), the all-sky TOA RSR (F_{TOA}^{\uparrow}) can be decomposed into the atmospheric and surface components (RSR_{atm} and RSR_{surf}).

$$F_{TOA}^{\uparrow} = RSR_{surf} + RSR_{atm} \quad (8)$$

The simplified calculation equations are as follows (Li et al., 2025):

200
$$RSR_{atm} = \frac{S(SF_{TOA}^{\uparrow} - F_S^{\uparrow}F_S^{\downarrow})}{S^2 - F_S^{\uparrow 2}} \quad (9)$$

$$RSR_{surf} = F_{TOA}^{\uparrow} - RSR_{atm} = F_{TOA}^{\uparrow} - \frac{S(SF_{TOA}^{\uparrow} - F_S^{\uparrow}F_S^{\downarrow})}{S^2 - F_S^{\uparrow 2}} \quad (10)$$

where S is the incident solar radiation at TOA, F_{TOA}^{\uparrow} is the RSR at TOA, and F_S^{\uparrow} and F_S^{\downarrow} represent the upwelling and downwelling shortwave radiation fluxes at the surface, respectively. Similarly, the clear-sky RSR ($F_{TOA,clr}^{\uparrow}$) can be decomposed into
205 $RSR_{surfclr}$ and RSR_{atmclr} .

$$F_{TOA,clr}^{\uparrow} = RSR_{surfclr} + RSR_{atmclr} \quad (11)$$

The cloud component RSR_{cloud} is defined as the difference in the atmospheric component of RSR between all-sky and clear-sky conditions:

$$RSR_{cloud} = RSR_{atm} - RSR_{atmclr} \quad (12)$$

210 This quantity represents the solar radiation directly reflected by clouds themselves. Its magnitude and variability are primarily determined by the CF and CR. Notably, RSR_{cloud} is distinct from the traditional shortwave cloud radiative forcing at TOA ($SWCRF_{TOA}$), which also includes the effect of clouds masking the surface-reflected component. The $SWCRF_{TOA}$ is defined as the difference in TOA RSR between all-sky
215 and clear-sky conditions:

$$SWCRF_{TOA} = F_{TOA}^{\uparrow} - F_{TOA,clr}^{\uparrow} \quad (13)$$

The relationship between the RSR_{cloud} and the $SWCRF_{TOA}$ can be derived by substituting the decompositions:



$$\begin{aligned}
 SWCRF_{TOA} &= (RSR_{surf} + RSR_{atm}) - (RSR_{surfclr} + RSR_{atmclr}) \\
 &= (RSR_{atm} - RSR_{atmclr}) + (RSR_{surf} - RSR_{surfclr}) \\
 &= RSR_{cloud} + F_{mask}
 \end{aligned} \tag{14}$$

220 where $F_{mask} = RSR_{surf} - RSR_{surfclr}$ represents the cloud masking effect on surface-reflected radiation—i.e., the reduction in TOA upwelling shortwave flux caused by clouds obscuring the surface.

Therefore, RSR_{cloud} can be equivalently expressed as the difference between the shortwave cloud radiative effect at TOA and this masking effect. Using the decomposition of $SWCRF_{TOA}$ into contributions from nine cloud types (Equation 1), we have:

$$RSR_{cloud} = SWCRF_{TOA} - F_{mask} = \sum_{c=1}^9 (CF_c \times CR_c) - F_{mask} \tag{15}$$

Where CF_c and CR_c are the cloud fraction and intrinsic cloud radiative effect for cloud type c , respectively.

230 Thus, the monthly anomalies of grid RSR_{cloud} can be decomposed as follows:

$$\Delta RSR_{cloud} = \sum_{c=1}^9 (\Delta CF_c \times \overline{CR_c} + \Delta CR_c \times \overline{CF_c} + \Delta CF_c \times \Delta CR_c) - \Delta F_{mask} \tag{16}$$

The first two terms on the right-hand side represent the anomalies in RSR_{cloud} driven by changes in CF and CR, respectively, and the third term is their co-variation. The fourth term, $-\Delta F_{mask}$, represents the anomalies in RSR_{cloud} arising from changes in the cloud masking effect (ΔF_{mask}). It is important to note that the cloud masking effect (ΔF_{mask}) is intrinsically tied to changes in CF and CR. Building on this decomposition, we can further investigate the sources of trends in RSR_{cloud} across different latitudinal zones. Note that in Fig. 4c, we plot the trends in $-\Delta F_{mask}$ term but not ΔF_{mask} to show its contribution to ΔRSR_{cloud} trends.

240 It is important to clarify that $SWCRF_{TOA}$ used here differs from the surface shortwave cloud radiative effect (SW_{cld}^{\downarrow}) employed in Section 2.3 to compute the cloud contribution to T_s trends; the latter is a surface flux quantity. $SWCRF_{TOA}$ is used here solely for decomposing RSR_{cloud} and is not employed in subsequent analyses.

2.5 Quantifying Meteorological Contributions to Cloud Fraction Anomalies

245 To investigate the drivers of observed CF trends, we perform a stepwise multiple linear regression linking monthly CF anomalies for each cloud type to a set of relevant



cloud-controlling variables. The cloud-controlling factors for low-level clouds have been extensively discussed in previous studies (Qu et al., 2015; Klein et al., 2018; Scott et al., 2020; Andersen et al., 2022; Naud et al., 2023; Li et al., 2025; Naud et al., 2025), and those for high clouds have also been examined (Kemsley et al., 2024). In contrast, studies focusing on the controlling factors for middle-level clouds remain limited. Therefore, we select a set of candidate factors for middle clouds from dynamical, thermodynamical, and microphysical perspectives. Based on established physical understanding of cloud formation and dissipation, we select a set of cloud-controlling factors for each cloud height category (low, middle, and high clouds) as shown in Table 1. The detailed physical basis and calculation method for each variable selection is presented in Appendix A. All meteorological variables used in the calculations are derived from monthly mean ERA5 pressure-level data, while AOD is obtained from MERRA-2 monthly mean products.

Table 1. Cloud Controlling Factors for Low, Middle, and High Clouds.

Cloud Category	Cloud-controlling factors
Low clouds (Cu, Sc, St)	T_s ; Estimated inversion strength (EIS); 850 hPa vertical velocity (ω_{850}); Surface temperature advection (ST_{adv}); 10 m wind speed ($wind_{10}$); Sensible heat flux (SHF); 700 hPa relative humidity (RH_{700}); M parameter (M); Aerosol optical depth (AOD)
Middle clouds (Ac, As, Ns)	500 hPa vertical velocity (ω_{500}); RH_{700} ; Convective available potential energy (CAPE); 500 hPa vapor pressure deficit (VPD_{500}); Mid-tropospheric static stability (MTS); 700 hPa moisture flux convergence (MFC_{700}); 700 hPa temperature advection ($Tadv_{700}$); AOD
High clouds (Ci, Cs, Cb)	T_s ; 300 hPa vertical velocity (ω_{300}); RH_{700} ; Upper-tropospheric relative humidity (UTRH); Upper-tropospheric static stability (SUT); 300-hPa zonal wind shear (ΔU_{300}); CAPE; Tropopause temperature (T_{trop}); 300–700 hPa thickness (Thick); AOD

For each grid cell and cloud type, we regress the deseasonalized CF anomaly against the corresponding set of meteorological variables using a stepwise procedure. The regression model is:

$$\Delta CF_c(x, t) = \beta_0(x) + \sum_{k=1}^K \beta_k(x) \cdot \Delta V_k(x, t) \quad (17)$$



where ΔCF_c is the monthly CF anomaly for cloud type c at location x and time t ,
265 ΔV_k are the deseasonalized meteorological variables, β_k are the regression
coefficients, and β_0 is the intercept. The stepwise procedure is implemented with an
entry significance level of $p < 0.05$ and a removal significance level of $p < 0.10$, ensuring
that only variables with statistically meaningful explanatory power are retained. All
predictors are standardized prior to regression, while the dependent variable (CF
270 anomaly) remains unstandardized. Thus, the resulting coefficients represent the change
in CF per unit standard deviation change in each predictor.

After obtaining the standardized coefficients β_k for each grid cell and cloud type,
we compute the contribution of each meteorological variable to the CF anomaly at each
month as:

$$275 \quad \text{Contrib}_k(x, t) = \beta_k(x) \cdot \Delta V_k(x, t) \quad (18)$$

This quantity represents the portion of the CF anomaly that can be attributed to
variations in the k -th meteorological factor. For each of the six latitude zones, cloud
type, and meteorological variable, we compute the area-weighted zonal mean
contribution at each month. For each resulting zonal-mean time series, we then estimate
280 the linear trend ($\% \text{ decade}^{-1}$) using ordinary least squares, representing the contribution
of each meteorological factor to the long-term CF trend in that latitude zone.

3 Results and Discussion

3.1 Surface Warming Trends and the Radiative Contribution from Clouds

Figure 1a shows the global and latitude-zone averaged T_s warming trend along
285 with the T_s trends caused by changes in the surface shortwave and longwave cloud
radiative forcing. Note that the latitudinal-mean values are area-weighted, and thus the
sum of the zonal trends constitutes the global trend. From 2002 to 2023, the global
average T_s rose significantly by 0.22 K per decade. While the fastest warming occurred
in the high-latitudes of the Northern Hemisphere (NH) (Fig. S2), the NH mid-latitudes
290 contributes most to the global warming trend (Fig. 1a), primarily over Europe, the North
Pacific, and the western Atlantic off the southeastern coast of North America (Fig. S2).

Previous research emphasized the role of longwave radiation in surface warming,
particularly from greenhouse gases like water vapor. While clouds also contribute to
the greenhouse effect by absorbing and re-emitting longwave radiation (Arking, 1991),



295 cloud changes over the past two decades have induced a longwave cooling effect on T_s
 trends (Fig. 1a). This implies that the longwave effects alone are inadequate to
 accurately understand clouds' full radiative contribution to T_s trends. In fact, the
 radiative influence of clouds on the surface is twofold, involving longwave warming
 and shortwave cooling effects (Arking, 1991; Hartmann and Doelling, 1991; Wood,
 300 2012). Changes in cloud properties also modify the amount of shortwave radiation
 reflected by clouds, thereby influencing the solar radiation reaching the surface.
 Although the surface longwave warming effect has weakened, the shortwave cooling
 effect has diminished even more markedly. Consequently, clouds have exerted a strong
 positive (warming) shortwave contribution that outweighs the negative longwave
 305 contribution, leading to a net enhancement of the global T_s trend, with notable
 latitudinal differences (Fig. 1a). Globally, the opposing shortwave and longwave cloud
 contributions largely cancel, resulting in a modest net cloud-induced warming of
 approximately 0.013 K per decade (derived from the sum of CRC_{sw} and CRC_{lw} in Fig.
 1a). This suggests that non-cloud components—such as clear-sky greenhouse gas
 310 forcing—are the primary drivers of the global mean T_s trend.

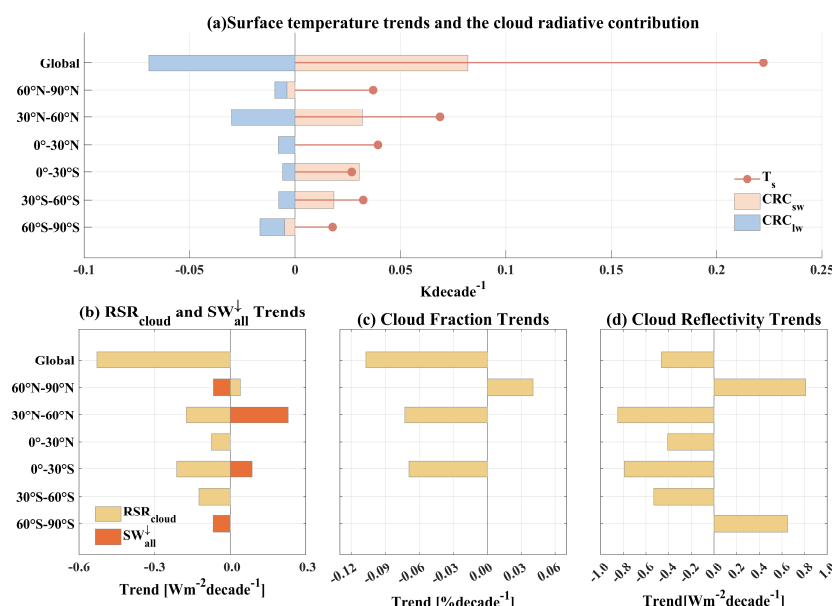


Figure 1. (a) ERA5 T_s trends from July 2002 to February 2023 and the T_s trends caused by changes in surface shortwave and longwave cloud radiative forcing (CRC_{sw} and CRC_{lw}) (methodology detailed in Section 2.3). (b) Global and latitude-zone averaged trends in the all-sky surface downward shortwave radiation fluxes (SW_{all}^{\downarrow}) and the cloud



component of TOA RSR (RSR_{cloud}), (c) CF, and (d) CR. Note that the latitudinal-mean trends in (a)-(c) are weighted by their area to account for their contributions to the global mean; the sum of the zonal trends approximately equals the global trend. Only trends significant at the 95% confidence level are shown.

320 However, the near-cancellation at the global scale belies the critical role of clouds
in affecting the spatial patterns of warming. The individual shortwave and longwave
cloud effects represent large, opposing radiative perturbations, and understanding their
separate drivers is essential for diagnosing cloud feedback mechanisms. At low and
mid-latitudes, these effects compete: changes in CRC_{sw} enhance surface warming,
325 while the CRC_{lw} partially offset it. Notably, in the Southern Hemisphere (SH) low
latitudes, the CRC_{sw} trend even exceeds the total T_s warming trend, which is partially
offset by a negative CRC_{lw} trend. In the mid-latitudes of both hemispheres, the trends
in the CRC_{sw} account for 57% (SH) and 47% (NH) of their T_s warming trend,
underscoring its important role in the warming. In contrast, at high latitudes, the effects
330 combine, as both cloud shortwave and longwave effects contribute to negative T_s trends,
indicating that cloud changes partially mitigate polar warming (Alkama et al., 2020).
Therefore, while the global net cloud impact on the T_s trend is small, clouds exert a
powerful and spatially heterogeneous influence that is fundamental to understanding
the observed pattern of climate change.

335 To further investigate the drivers of cloud-induced T_s trends, Fig. 1b shows the
global and latitude-zone averaged trends in surface downwelling shortwave radiation
under all-sky condition (SW_{all}^{\downarrow}). While the SW_{all}^{\downarrow} directly affects surface energy
balance, its changes are fundamentally governed by cloud-induced changes in RSR at
the TOA. We therefore also examine the trends in cloud component of TOA RSR
340 (RSR_{cloud}) (Fig. 1b) and its key drivers—CF (Fig. 1c) and CR (Fig. 1d). In 30–60°N and
0–30°S, the shortwave warming contribution from clouds (Fig. 1a) is primarily due to
significant increased solar radiation reaching the surface (Fig. 1b), resulting from
reduced RSR_{cloud} (Fig. 1b), which is driven by both decreased CF (Fig. 1c) and reduced
CR (Fig. 1d). This finding is consistent with Goessling et al. (2024), who highlighted
345 that the recent decline in PA, particularly the record-low value in 2023, was
predominantly driven by reduced low-level cloud cover over NH mid-latitudes and
tropics, substantially amplifying global warming. In 0–30°N, although decreased CR
leads to significantly less RSR_{cloud} , the solar radiation reaching the surface shows no
significant increase (Fig. 1b), likely due to enhanced absorption by atmospheric water



350 vapor (Loeb et al., 2021). Consequently, the shortwave cloud contribution to T_s trends is not significant here (Fig. 1a). Differently, in 30–60°S, despite no significant trend in SW_{all}^{\downarrow} (Fig. 1b), clouds exhibit a substantially positive shortwave contribution to the T_s trend (Fig. 1a). This is because a decrease in RSR_{cloud} driven by reduced CR contributes to an increase in solar radiation reaching the surface, which offset the decrease in surface downwelling solar radiation caused by increased aerosol reflection and atmospheric water vapor absorption (Fig. S3b; Li et al., 2024b). Therefore, clouds exert a positive shortwave contribution to T_s trends by counteracting this aerosol-driven cooling. Conversely, at high latitudes, increased CF and enhanced CR result in more solar radiation being reflected, reducing the solar radiation reaching the surface (Fig. 360 1b) and thereby partially mitigating surface warming.

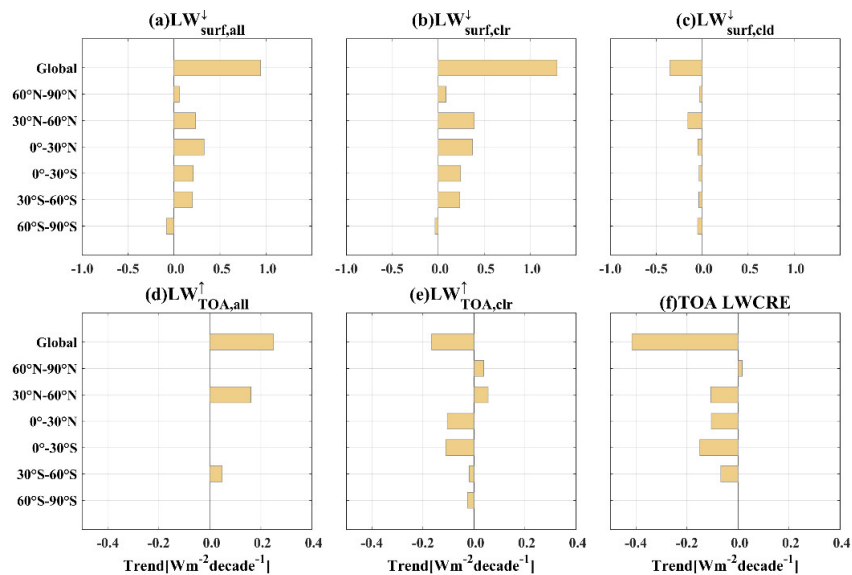


Figure 2. Global and latitude-zone averaged trends in longwave radiation fluxes from July 2002 to February 2023. (a) All-sky surface downward longwave radiation ($LW_{surf,all}^{\downarrow}$), (b) clear-sky surface downward longwave radiation ($LW_{surf,clr}^{\downarrow}$), and (c) the difference between all-sky and clear-sky conditions ($LW_{surf,clr}^{\downarrow} - LW_{surf,all}^{\downarrow}$). (d) All-sky TOA outgoing longwave radiation ($LW_{TOA,all}^{\uparrow}$), (e) clear-sky TOA outgoing longwave radiation ($LW_{TOA,clr}^{\uparrow}$), (f) TOA longwave cloud radiative effect (TOA LWCRE = $LW_{TOA,clr}^{\uparrow} - LW_{TOA,all}^{\uparrow}$). Note that latitudinal-mean trends are area-weighted to account for their contributions to the global mean; the sum of the zonal trends approximately equals the global mean. Only trends significant at the 95% confidence level are shown. 370

Concurrently, changes in cloud properties also drive trends in the longwave cloud



contribution to T_s trends (CRC_{lw}). Fig. 2 shows the trends in surface and TOA longwave radiation fluxes. In the 30–60°N and 0–30°S regions, although clear-sky components
375 (e.g., water vapor and greenhouse gases) lead to an increasing trend in surface downward longwave radiation (Fig. 2b), the significant decrease in CF (Fig. 1c) causes the cloud-induced change in surface downward longwave radiation (i.e., the difference between all-sky and clear-sky; Fig. 2c) to exhibit negative trends. This indicates a weakened cloud greenhouse effect, allowing more surface heat to escape to space and
380 thereby partially offsetting surface warming (Fig. 1a). Similarly, Liu et al. (2025) identified a widespread negative longwave cloud feedback over low- and mid-latitude continents, where declining low-level cloud cover reduces downwelling longwave radiation and partially mitigates surface warming. However, in the NH high latitudes, despite a significant increase in total CF, the cloud-induced change in surface downward
385 longwave radiation shows a decreasing trend (Fig. 2c), which can be explained by a shift in cloud vertical structure. Since the downwelling longwave emission from clouds depends largely on cloud base height (Viúdez-Mora et al., 2015), the observed trend may stem from a decrease in low-level clouds (which emit more) and an increase in high-level clouds (which emit less). At the TOA, the outgoing longwave radiation (OLR)
390 trends (Figs. 2d–f) further support these interpretations. Over 30–60°N and 0–30°S, the reduction in CF allows more longwave radiation to escape to space, resulting in an increase in outgoing longwave radiation, corresponding to a negative TOA longwave cloud radiation effect trend. In contrast, over the NH high latitudes, the increase in high clouds (with colder cloud tops) reduces the OLR emitted to space. Overall, changes in
395 CF and cloud vertical distribution jointly drive the longwave cloud radiative effects on T_s trends.

3.2 The Key Role of Cloud Transition and Its Potential Mechanisms

Given the distinct radiative properties of clouds at different altitudes and optical depths (Hartmann et al., 1992), systematic shifts in their distribution and characteristics
400 significantly influence the cloud radiative effects and their contribution to T_s trends. The signal of these changes, however, is often masked within analyses of total cloud properties. To clarify this issue, we first examine the observed trends in CF and CR across nine cloud types (Fig. S4). These trends vary substantially between land and ocean (Fig. 3). We then quantify how these CF and CR changes affect the reflected solar



405 radiation by clouds (RSR_{cloud}). Fig. 4 displays the global and latitude-zone averaged
 RSR_{cloud} trends driven by changes in CF and CR across nine cloud types.

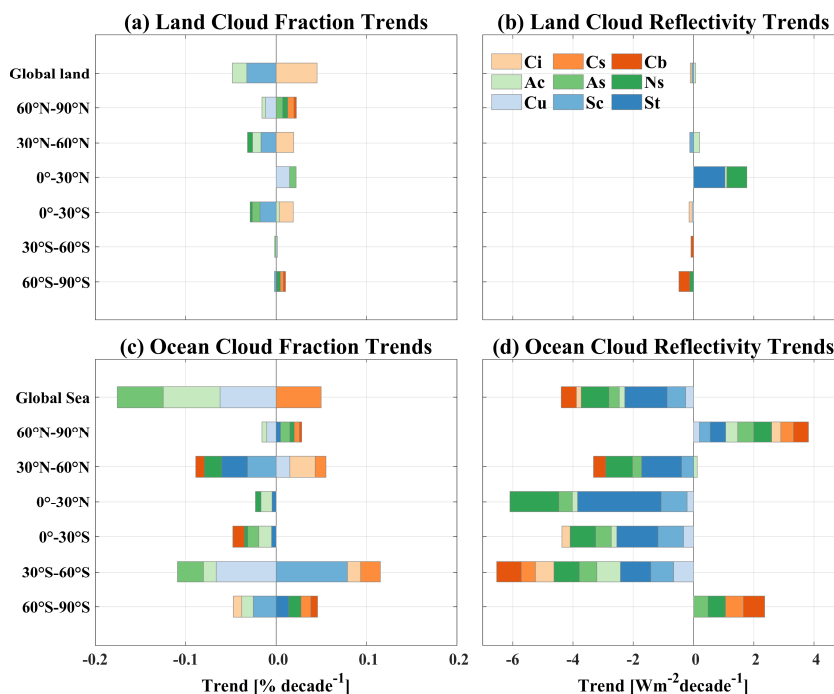
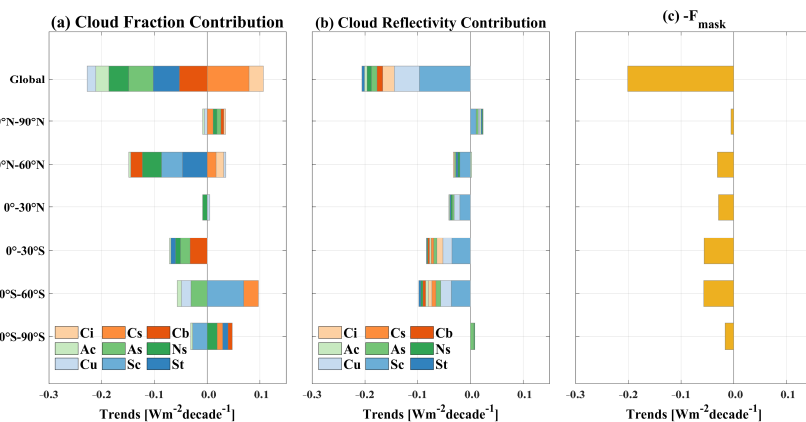


Figure 3. Latitude-zone and global averaged trends (2001–2024) for CF and CR over (a-b) lands and (c-d) oceans. The CF trends for each zone are area-weighted to represent global contributions. Only trends significant at the 95% confidence level are shown.

Globally, the decline in RSR_{cloud} is predominantly driven by the reduced CR, with the CF playing a secondary role (Fig. 4a, 4b). Specifically, the global RSR_{cloud} reduction trend of $-0.22 \text{ Wm}^{-2}\text{decade}^{-1}$ (the sum of contributions from all cloud types, including non-significant ones) is attributed to the cumulative decrease in CR of most cloud types (Fig. 4b), whereas the reduction of $-0.14 \text{ Wm}^{-2}\text{decade}^{-1}$ arises from compensating CF changes among different cloud types (Fig. 4a). This is largely due to a systematic cloud regime change: a shift from low-level (St and Cu), mid-level, and Cb clouds toward high-level optically thin clouds (Cs and Ci). As a result, the negative RSR_{cloud} contributions from the displaced low-level, mid-level, and Cb clouds are partially offset by the positive contributions from the increasing high-level optically thin clouds. This transition, characterized by a rising cloud base height, would also reduce the downwelling longwave emission from clouds to the surface, thereby confirming the



observed longwave cooling contribution of clouds to the T_s trend (Fig. 1a). The potential role of cloud masking effects will be discussed later in this section.



425

Figure 4. The trends in domain-averaged RSR_{cloud} caused by the changes in (a) CF and (b) CR across nine cloud types, and (c) the cloud masking effect ($-\Delta F_{mask}$), at global and latitudinal scales, sorted in descending order of magnitude. Note that the latitudinal-mean trends are weighted by their area to account for their contributions to the global mean; the sum of the zonal trends approximately equals the global trend. Only trends significant at the 95% confidence level are shown.

430

To understand the drivers of the observed CF trends, we perform a stepwise multiple linear regression linking monthly CF anomalies to a set of cloud-controlling factors (Table 1). The temporal correlation coefficient between observed and regressed CF anomalies exceeds 0.6 for Cu, Sc, As, Ci, Cs, and Cb over mid- and low-latitude oceans, and reaches above 0.9 in the tropics (Fig. S5). For other cloud types, the correlation remains above 0.5 in regions where they are climatologically prevalent, indicating reasonable explanatory power. The contributions of each factor to the CF trend are calculated at the grid-cell level (by multiplying the regression coefficient by the local factor trend) and then area-weighted to zonal means. For clarity, we have only presented the zonal-mean coefficients and factor trends as shown in Fig. S6 and Fig. 5, respectively. Figure 6 shows the area-weighted contributions of individual factors to the CF trend across nine cloud types and six latitude zones. Black circles denote the observed CF trend, and red circles denote the sum of all factor contributions. The close agreement between black and red circles indicates that the model captures a reasonable portion of the trends. However, the underlying mechanisms are more complex, and the statistical relationships should not be overinterpreted as a complete physical explanation, particularly for mid-level mixed-phase clouds. Nonetheless, the close

445



agreement in Fig. 6 suggests that the selected factors represent the dominant large-scale
 450 drivers, especially for cloud types that dominate the RSR_{cloud} decline.

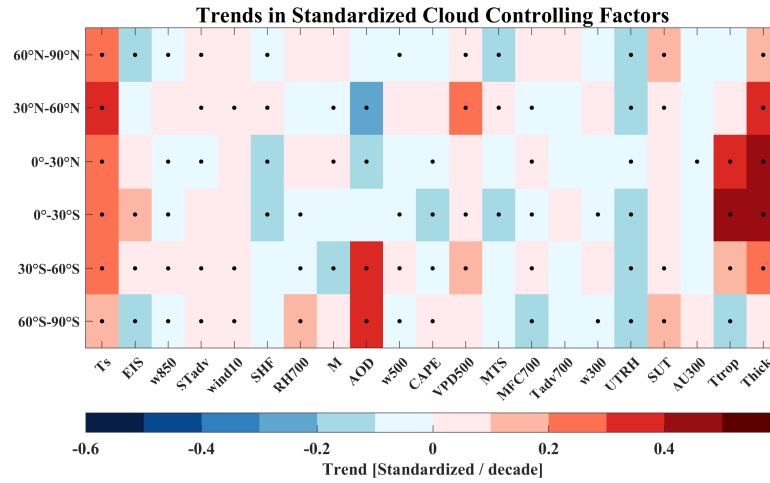


Figure 5. Decadal trends of standardized cloud controlling factors over the period 2002–2023 (units: per decade). Black dots indicate trends that are statistically significant at the 95% confidence level ($p < 0.05$). The factor list includes all variables considered for low-, mid-, and high-level cloud analyses.
 455

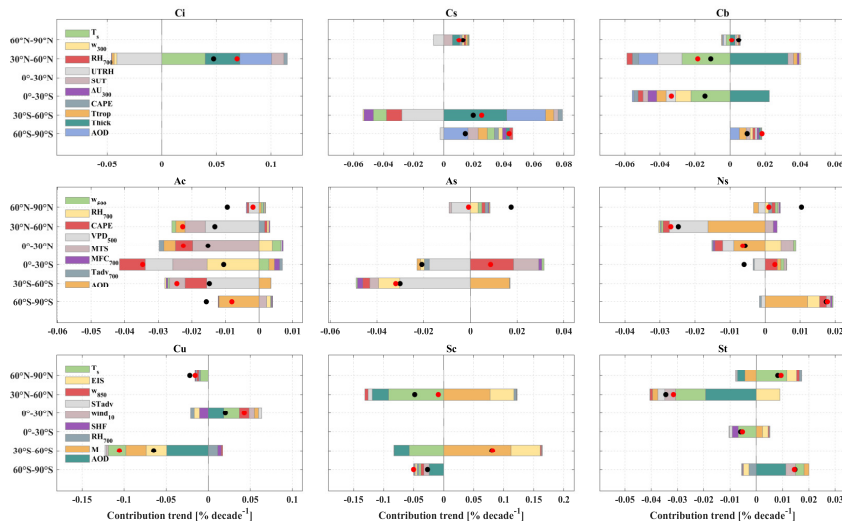


Figure 6. Contributions of meteorological factors to CF trends ($\% \text{ decade}^{-1}$) for nine cloud types across six latitude zones, sorted in descending order of magnitude. Black dots indicate the observed significant CF trend, while red dots denote the sum of factor contributions. Latitudinal means are area-weighted to account for their contributions to the global mean. Only trends significant at the 95% confidence level are highlighted.
 460

In contrast, the trends in CR are not explicitly regressed against meteorological



factors, as CR is more directly linked to cloud microphysical properties. Fig. 7 presents the zonal-mean trends in CVOD and particle radii (r_{liq} , r_{ice}), which serve as the primary
 465 controls on CR and provide complementary insights into the mechanisms underlying the RSR_{cloud} changes.

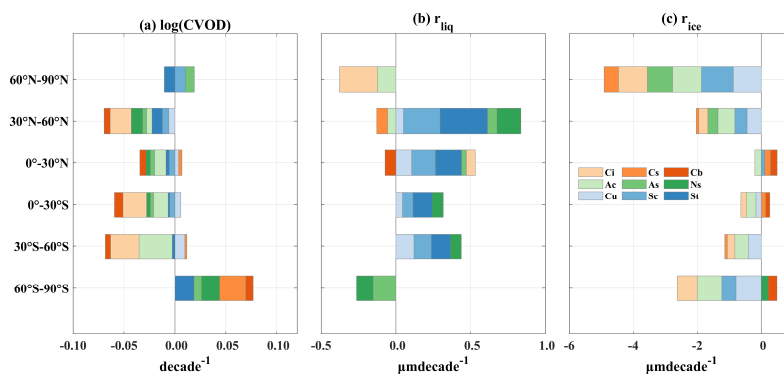


Figure 7. Latitude-zone averaged trends in cloud properties (July 2002–February 2023) for (a) logarithm of cloud visible optical depth (log CVOD), (b) liquid cloud particle radius (r_{liq}), and (c) ice cloud particle radius (r_{ice}). Only trends significant at the 95% confidence level are shown.
 470

The most pronounced reductions in CF contributions occur in the NH mid-latitudes and the SH low latitudes (Fig. 4a). In the NH mid-latitudes, these decreases are most pronounced over the oceans (Fig. 3), mainly attributed to St, Sc, Ns, and Cb.
 475 The CF decline of St and Sc, which contribute most to the reduction in RSR_{cloud} , is largely explained by rising T_s and decreasing AOD (Fig. 5, Fig. 6). The warming-induced suppression of low clouds is consistent with the positive cloud–temperature feedback mechanisms (Klein et al., 2018; Myers et al., 2018), while the reduction in AOD implies fewer cloud condensation nuclei (CCN), further inhibiting cloud
 480 formation. For Ns, the decreasing trend is mainly attributed to reduced AOD and increased mid-tropospheric dryness, as indicated by the positive VPD_{500} trend. The higher VPD reflects lower relative humidity and less saturated conditions, making it harder for cloud droplets to form and persist, thereby inhibiting cloud growth. The decline in Cb is jointly driven by decreasing UTRH, and reduced AOD, while the
 485 increase in tropospheric thickness partially offsets this decline. Although the zonal-mean attribution suggests a substantial contribution from T_s (Fig. 6), this relationship is primarily evident over land (not shown), whereas the dominant decrease in Cb occurs over oceanic regions (Fig. 3). Therefore, increasing T_s is unlikely to be a direct driver



of the oceanic Cb reduction. Furthermore, the decreases in Ns and Cb may be linked to
490 large-scale circulation adjustments under global warming. Model projections have
suggested that in a warmer climate, baroclinic activity in the NH mid-latitudes may
weaken due to Arctic amplification (Hadas et al., 2023). As a result, the frequency and
intensity of mid-latitude cyclones are expected to diminish, thereby weakening large-
scale ascent and consequently implying cloud reductions. Moreover, Tselioudis et al.
495 (2025) also provide observational evidence of a continuous contraction of mid-latitude
storm cloud regions over the past 24 years.

In the SH low latitudes, the largest contribution to the RSR_{cloud} decrease comes
from the reduction in Cb, followed by Ns, As, and St. The reduction in Cb is primarily
controlled by decreasing trends in upper-level ascent (as indicated by ω_{300}), reduced
500 UTRH, and increasing trends in tropopause temperature. Similar to the NH mid-
latitudes, the T_s signal in the zonal-mean attribution is dominated by land, while the
observed Cb reduction is primarily oceanic. Moreover, although the zonal-mean ω_{300}
exhibits a downward trend (Fig. 5)—suggesting a weakening of large-scale uplift—the
spatial pattern derived from multiple linear regression reveals that the negative
505 contribution of ω_{300} to Cb is concentrated over the western equatorial Pacific, where
 ω_{300} actually shows a significant upward trend locally (not shown). This may be
associated with a weakening of the Walker circulation (Wu et al., 2021) over the western
equatorial Pacific, which suppresses convective development and moisture uplift,
limiting the formation of these clouds. In summary, the decline in Cb over 0-30°S
510 is more robustly explained by dynamical weakening (reduced ascent and moisture supply)
and upper-tropospheric thermodynamic changes (increased tropopause temperature and
drying), which suppress deep convection and limit cloud development. Notably, the
CF's contribution to the RSR_{cloud} trend is much smaller in the SH mid-latitudes than in
its northern counterpart (Fig. 4). This can be attributed to a systematic shift from Cu to
515 the more reflective Sc, which compensates for the RSR_{cloud} decrease caused by reduced
mid-level clouds. As shown in Fig. 6, the increasing EIS trend and decreasing instability
(M parameter) trend suppress convective Cu while favor the formation of the more
stable Sc.

The decrease in RSR_{cloud} contributed by reduced CR is primarily concentrated in
520 the mid- to low-latitudes, particularly across the SH, with the Sc contributing most
significantly (Fig. 4b). In both the SH low latitudes and NH mid- to low-latitudes, the



diminished reflectivity of Sc can be attributed to significant decrease in its CVOD (Fig. 7a). Furthermore, a pronounced increase in the r_{iq} over mid- and low-latitude regions reduces the total scattering surface area of cloud droplets, resulting in less RSR (Fig. 7b). In addition, the decline in CR in the NH mid-latitudes is also potentially linked to reduced aerosols following controls on industrial and shipping sulfur emissions (Fig. 5). This reduction in CCN leads to decreased cloud droplet number concentrations and larger effective droplet radii (Fig. 7b), thereby lowering cloud albedo (Li et al., 2018; Cao et al., 2023; Hodnebrog et al., 2024; Yuan et al., 2024; Li et al., 2025). Similarly, Bai et al. (2020) have reported a persistent decline in both cloud droplet number concentration and AOD along the east coast of the United States, the west coast of Europe, and the east coast of China from 2003 to 2017. Moreover, von Salzen et al. (2025) have observed that the decrease in marine CR over the North Atlantic and Northeast Pacific from 2003 to 2022 can be attributed to the reduction in sulfur dioxide and other aerosol precursors. Notably, across SH low and mid-latitudes, a reduction in CR across nearly all cloud types has significantly contributed to the negative trend in RSR_{cloud} , which is consistent with their significant reduction in CVOD (Fig. 7a). This widespread darkening of clouds occurs despite increasing AOD in the SH mid-latitudes (Fig. 5), suggesting that the rising aerosol burden has not been efficiently translated into CCN (Cao et al., 2023). This is likely because the increased AOD is dominated by natural aerosols (e.g., sea salt) and above-cloud smoke, which are less effective as CCN or reside above the cloud layer, limiting their influence on boundary-layer clouds (Cao et al., 2023).

In contrast to the low- to mid-latitudes, increased CF and enhanced CR have led to a rise in RSR_{cloud} , thereby mitigating regional warming in the high latitudes of both hemispheres (Fig. 4a, b). The increase in CF is primarily attributed to optically thick mid- and high-level clouds. Although the model's performance is relatively limited at high latitudes (Fig. S5), it still captures some of the physical processes. In the NH high latitudes, the positive trend in high clouds (Cs) is mainly linked to enhanced SUT and increased tropospheric thickness. For mid-level clouds (Ns), the increasing trend is primarily associated with enhanced mid-tropospheric moisture supply (RH_{700}) and strengthened warm advection ($Tadv_{700}$), which promote large-scale ascent and stratiform cloud formation. In the SH high latitudes, the increase in Ns is primarily driven by positive trends in AOD, RH_{700} , and CAPE, indicating the combined effects



555 of increased CCN, enhanced moisture supply, and strengthened convective instability. The increase in high clouds (Cs and Cb) is associated with increasing AOD and SUT, along with decreasing T_{trop} . Additionally, the increase in St is linked to rising AOD and enhanced near-surface wind speed, which promote boundary-layer cloud formation through enhanced turbulent mixing. These statistically derived relationships are
560 consistent with large-scale environmental changes in the polar regions. Enhanced atmospheric moisture (Ding et al., 2022; Patel and Kuttippurath, 2023) stems from intensified evaporation due to a wider ocean surface resulting from sea ice retreat (He et al., 2019) and increased poleward moisture transport from lower latitudes (Woods and Caballero, 2016; Kim et al., 2017), creating conditions more favourable for cloud
565 development. This process is further amplified by the poleward shift of cyclone and storm tracks, which brings extensive cloud systems to the polar region (Tselioudis et al., 2024). Simultaneously, the observed cloud transition, characterized by a decrease in high-emissivity low-level clouds and an increase in low-emissivity high-level clouds, provides the key to understanding the longwave cloud contribution to polar T_s trends.
570 This shift explains why the longwave cloud radiative effect has weakened, contributing negatively to the surface warming trend in both polar regions (Fig. 1a), despite the increased total CF in the NH and the stable total CF in the SH (Fig. 1c).

Moreover, the increase in CR at high-latitudes is mainly driven by low- and mid-level clouds in the NH and mid-level clouds in the SH. This enhancement is largely due
575 to a significant increase in CVOD (Fig. 7a), likely resulting from greater moisture availability and elevated in-cloud liquid water content. Satellite observations have revealed that, over the past two decades, Arctic clouds have shown a tendency to shift from the ice to the liquid phase, with increased liquid water content enhancing cloud albedo (Lelli et al., 2023). Additionally, the expansion of open ocean area enhances
580 emissions of sea salt and biogenic aerosols, increasing the availability of cloud condensation and ice nuclei (Fig. 7c) (Schmale et al., 2021; Twohy et al., 2021; Lapere et al., 2023). This promotes higher cloud droplet number concentrations and reduces droplet size (Fig. 7b, 7c), contributing to brighter and longer-lasting clouds.

It is noteworthy that the contribution of CF and CR changes to the trend in RSR_{cloud}
585 also encompasses the masking effect of clouds on surface-reflected radiation (ΔF_{mask}). The total contribution of this effect to RSR_{cloud} trends ($-\Delta F_{\text{mask}}$), defined as the difference of the TOA RSR surface component between clear-sky and all-sky



conditions, is shown in Fig. 4c (see Section 2.4 for detailed explanation). This term (typically positive) exhibits a significant negative trend, which likely arises from two interrelated surface-cloud processes: first, a reduction in surface albedo due to declining snow/ice cover (Wu et al., 2020) or vegetation greening (Chen et al., 2019) lowers the clear-sky surface reflection (Li et al., 2024b), thereby diminishing the potential masking effect of clouds; second, a decrease in CF or a reduction in CR directly weakens the masking intensity by allowing more surface-reflected radiation to escape under cloudy conditions.

4 Conclusions

Driven by the ongoing climate crisis, this study quantifies the cloud radiative contribution to surface warming (2002-2023) using surface energy balance equation and CERES data. Globally, cloud changes cause shortwave warming, partly offset by longwave cooling. This stems from a systematic cloud regime transition from low-/mid-level and Cb clouds toward high-level optically thin clouds (Cs, Ci), which is driven by large-scale circulation adjustments (Tselioudis et al., 2025), thermodynamic feedbacks (Klein et al., 2018), and microphysical processes (Li et al., 2018). This shift explains the reduction in the cloud component of PA and the decrease in longwave radiation emitted by clouds towards surface.

Regionally, the mechanisms exhibit hemispheric difference. In 30–60°N, the RSR_{cloud} decline stems mainly from reduced CF (especially St, Sc, Ns, and Cb), which is consistent with rising SSTs, reduced AOD, and mid-tropospheric drying. In contrast, in 30–60°S, it is mainly driven by reduced CR, partially mitigated by increased CF resulting from enhanced atmospheric stability that promote a shift from Cu to Sc, along with increased Cs. This mechanistic difference limits interhemispheric PA compensation from mid-latitude clouds on short timescales, which is supported by Diamond et al. (2024) and Loeb et al. (2025). Moreover, in 0–30°S, decreased CF (high-/mid-level clouds) and reduced CR (low-level clouds) contribute equally, associated with weakened ascent velocity, upper-tropospheric drying, and decreased CVOD with increased τ_{liq} , respectively. Conversely, across both polar regions, clouds mitigate warming through both shortwave and longwave radiation changes, linked to increased CF and CR, particularly for mid/high clouds, resulting from increased water vapor, AOD, SUT, and enhanced CVOD.



620 The observed reductions in CF and CR are consistent with the long-term decline
in global PA reported over recent decades (Li et al., 2025). Looking forward, this trend
is projected to persist, with continued declines in RSR expected across the 21st century
under all emission scenarios, particularly under high-emission pathways where the rate
of decline accelerates (Li et al., 2025). These findings highlight that the cloud regime
625 shifts identified in this study not only contribute to current surface warming but also
imply a sustained reduction in PA that will amplify future climate change. Moreover,
given that subtropical low clouds dominate unforced interannual-to-decadal
fluctuations in global energy imbalance (Miyamoto et al. 2026), their projected long-
term decline under warming may not only amplify the forced energy uptake but also
630 modulate the amplitude of future internal variability.

It should be also noted, however, that our findings are derived from passive
satellite measurements, which have inherent limitations in distinguishing clouds from
aerosols and over highly reflective surfaces (Yamanouchi et al., 1987; King et al., 1992;
Mahesh et al., 2004), and cannot provide vertical cloud profile information. Future
635 research based on active satellite observations is necessary to advance the
understanding of cloud transition processes.

Appendix A. Cloud-controlling Factors and Variable Definitions

This appendix presents the full set of cloud-controlling factors used in the stepwise
multiple linear regression for low, middle, and high clouds. Table A1 lists the factors
640 for each cloud category along with their physical mechanisms.

Table A1. Cloud controlling factors for low, middle, and high clouds and their physical mechanisms.

Cloud Category	Cloud-controlling factors	Physical Mechanism
Low clouds (Cu, Sc, St)	Surface skin temperature (T_s ; K)	Modulates boundary-layer thermal structure and cloud-top entrainment rate.
	Estimated inversion strength (EIS; K)	Measures lower-tropospheric stability. See Eq. (A1) for details.
	850 hPa vertical velocity (ω_{850} , positive downward; Pa s ⁻¹)	Represents large-scale subsidence/upwelling in the lower troposphere.
	Surface temperature advection	Modulates lower-tropospheric stability



	$(ST_{adv}; K s^{-1})$	via horizontal temperature advection. See Eq. (A2) for details.
	10 m wind speed ($wind_{10}; m s^{-1}$)	Regulates surface turbulent fluxes affecting cloud formation.
	Sensible heat flux (SHF; $W m^{-2}$)	Contributes to boundary-layer heat budget and turbulent mixing.
	Relative humidity at 700 hPa ($RH_{700}; \%$)	Modulates dry-air entrainment at cloud top.
	M parameter (M; K)	The potential temperature difference between the surface and 800 hPa. Indicates boundary-layer instability and cold-air advection.
	Aerosol optical depth (AOD)	Influences cloud droplet number concentration and cloud lifetime.
Middle clouds (Ac, As, Ns)	500 hPa vertical velocity (ω_{500} , positive downward; $Pa s^{-1}$)	Represents mid-tropospheric large-scale ascent.
	RH_{700}	Indicates lower-to-mid tropospheric moisture supply.
	Convective available potential energy (CAPE; $J kg^{-1}$)	Reflects convective instability.
	500 hPa vapor pressure deficit ($VPD_{500}; kPa$)	Measures mid-level dryness controlling cloud dissipation. See Eq. (A3) for details.
	Mid-tropospheric static stability (MTS; K)	The potential temperature difference between 500 hPa and 700 hPa, representing mid-tropospheric static stability.
	700 hPa moisture flux convergence ($MFC_{700}; kg kg^{-1} s^{-1}$)	Quantifies horizontal moisture transport convergence. See Eq. (A5) for details.
	700 hPa temperature advection ($T_{adv700}; K s^{-1}$)	Represents thermal advection affecting cloud development. See Eq. (A6) for details.
	AOD	Influences cloud droplet number concentration and cloud lifetime.
High clouds (Ci, Cs, Cb)	T_s	Influences deep convection and upper-level cloud formation.
	300 hPa vertical velocity (ω_{300} , positive downward; $Pa s^{-1}$)	Represents upper-tropospheric dynamical forcing.
	RH_{700}	Low-to-mid tropospheric moisture modulates convective initiation.
	Upper-tropospheric relative	Defined as the vertically averaged



humidity (UTRH; %)	relative humidity within the 200 hPa layer below the tropopause. Indicates upper-tropospheric moisture availability.
Upper-tropospheric static stability (SUT; K km ⁻¹)	Represents upper-tropospheric static stability. See Eq. (A7) for details.
300-hPa zonal wind shear (ΔU_{300})	300 hPa zonal wind shear affects upper-level cloud organization. See Eq. (A8) for details.
CAPE	Controls deep convective intensity.
Tropopause temperature (T_{trop} ; K)	Sets upper bound on convective cloud top height and cirrus formation.
300–700 hPa thickness (Thick; m)	Calculated as the difference in geopotential height between 300 and 700 hPa; indicative of tropospheric mean temperature and thermal expansion.
AOD	Influences cloud droplet number concentration and cloud lifetime.

Estimating Inversion Strength (EIS) is calculated according to the formula:

$$EIS = LTS - \Gamma_m^{850}(Z_{700} - Z_{LCL}) \quad (A1)$$

where lower-tropospheric stability (LTS) is defined as the potential temperature difference between 700 hPa and the surface, Γ_m^{850} represents the moist adiabatic lapse rate at 850 hPa, and Z_{700} and Z_{LCL} denote the geopotential height at 700 hPa and the lifting condensation level relative to the surface, respectively. Following Wood and Bretherton (2006), the surface relative humidity is assumed to be 80% to simplify the estimation of surface dewpoint temperature, with Z_{LCL} computed following Georgakakos and Bras (1984).

Surface temperature advection (ST_{adv}) is computed as:

$$ST_{adv} = -\frac{u}{R_E \cos \varphi} \frac{\partial ST}{\partial \lambda} - \frac{v}{R_E} \frac{\partial ST}{\partial \varphi} \quad (A2)$$

where u and v denote eastward and northward 10-m winds, φ and λ represent latitude and longitude, R_E is the Earth's radius, and ST denotes the 2-m air temperature. Positive/negative ST_{adv} indicates warm/cold advection.

Vapor pressure deficit at 500 hPa (VPD_{500}) is defined as the difference between the saturation vapor pressure (SVP) and the actual vapor pressure (AVP) at 500 hPa (Murray, 1966; Buck, 1981):

$$VPD = SVP - AVP = SVP \times (1 - RH) \quad (A3)$$



$$SVP = 6.1078 \times e^{\frac{a \times T_a}{T_a + b}} \quad (A4)$$

660 Here RH is the relative humidity, T_a is the air temperature at 500 hPa. The constants a and b depend on the phase of water: for T_a at or above 0 °C (liquid water), a=17.27 and b=237.3; for T_a below 0 °C (ice), a=21.875 and b=265.5.

Moisture flux convergence at 700 hPa (MFC₇₀₀) is calculated as the negative divergence of the horizontal moisture flux:

$$665 \quad MFC_{700} = -\nabla \cdot (q\mathbf{V}) \quad (A5)$$

where q is specific humidity (kg kg⁻¹) and $\mathbf{V}=(u,v)$ the horizontal wind vector at 700 hPa. Convergence (positive MFC) indicates accumulation of moisture, which favors cloud formation.

Temperature advection at 700 hPa (Tadv₇₀₀) is given by:

$$670 \quad Tadv_{700} = -\frac{u_{700}}{R_E \cos \varphi} \frac{\partial T_{700}}{\partial \lambda} - \frac{v_{700}}{R_E} \frac{\partial T_{700}}{\partial \phi} \quad (A6)$$

where u_{700} and v_{700} denote eastward and northward wind components at 700 hPa, φ and λ represent latitude and longitude, R_E is the Earth's radius, and T_{700} is the air temperature at 700 hPa.

Upper-tropospheric static stability (SUT) is computed following the method 675 described by Kemsley et al. (2024). Temperature and pressure profiles are first interpolated to 100 vertical levels using cubic spline interpolation from standard pressure levels to resolve fine vertical gradients. At each interpolated pressure level p, the static stability S_p is calculated as

$$S_p = \frac{R_c T_p}{c_p p} - \frac{dT}{dp} \quad (A7)$$

680 where T_p is the temperature at pressure p, R_c is the gas constant, and c_p is the specific heat capacity at constant pressure. Finally, SUT is defined as the vertical average of S_p over the interpolated levels spanning from the tropopause pressure plus 50 hPa to the tropopause pressure plus 200 hPa. The tropopause pressure is identified on a monthly-mean basis using the standard World Meteorological Organization (WMO) 685 definition (Reichler et al., 2003).

300-hPa zonal wind shear (AU300) is defined as the vertical gradient of the zonal wind between 300 and 925 hPa (Kemsley et al. 2024):

$$\Delta U_{300} = \frac{U_{300} - U_{925}}{Z_{300} - Z_{925}} \quad (A8)$$



where U is the easterly wind speeds and z the geopotential height.

690

Data availability. All data used in this study are available to the public. The CERES_EBAF_Ed4.2.1 (Kato et al., 2018; Loeb et al., 2018; NASA/LARC/SD/ASDC, 2025) and FBCT Edition 4.1 (NASA/LARC/SD/ASDC, 2020; Sun et al., 2022) products are available through the NASA Langley Research Center CERES ordering
695 tool. The ERA5 datasets can be download through Climate Data Store (CDS) (Hersbach et al., 2023a; Hersbach et al., 2023b). The MERRA-2 datasets can be obtained from (Global Modeling and Assimilation Office, 2015; Buchard et al., 2017; Randles et al., 2017). All data are available in the main text or the supplementary materials.

Author contributions. RL organized the paper and performed related analysis. JL
700 conceptualized the paper and revised the whole manuscript. BJ, LZ, and JL modified the paper and provided suggestions for this study. All authors contributed to the discussion of the results and reviewed the manuscript.

Competing interests. The contact author has declared that none of the authors has any competing interests.

705 **Acknowledgments.** We would like to thank the CERES, MERRA-2, and ERA5 science teams for providing excellent and accessible data products that made this study possible.

Financial support. This work was jointly supported by National Key Research and Development Program of China (Grant No. 2024YFB3907900), the key Program of the National Natural Science Foundation of China (Grant No. 42430601), National Natural
710 Science Foundation of China (Grant No. 42305072), and Gansu Provincial Department of Education Outstanding Graduate Students “Innovation Star” Project (Grant No. 2025CXZX-075).

References

Alkama, R., Taylor, P. C., Garcia-San Martin, L., Douville, H., Duveiller, G., Forzieri,
715 G., Swingedouw, D., and Cescatti, A.: Clouds damp the radiative impacts of polar sea ice loss, *The Cryosphere*, 14, 2673-2686, <https://doi.org/10.5194/tc-14-2673-2020>, 2020.

Andersen, H., Cermak, J., Zipfel, L., and Myers, T. A.: Attribution of observed recent



- decrease in low clouds over the Northeastern Pacific to cloud-controlling factors,
720 Geophys. Res. Lett., 49, e2021GL096498,
<https://doi.org/10.1029/2021GL096498>, 2022.
- Andrews, T., Forster, P. M., and Gregory, J. M.: A surface energy perspective on climate
change, *J. Clim.*, 22, 2557-2570, <https://doi.org/10.1175/2008JCLI2759.1>, 2009.
- Arking, A.: The radiative effects of clouds and their impact on climate, *Bull. Am.*
725 *Meteorol. Soc.*, 72, 795-814, [https://doi.org/10.1175/1520-0477\(1991\)072%3C0795:TREOCA%3E2.0.CO;2](https://doi.org/10.1175/1520-0477(1991)072%3C0795:TREOCA%3E2.0.CO;2), 1991.
- Bai, H., Wang, M., Zhang, Z., and Liu, Y.: Synergetic satellite trend analysis of aerosol
and warm cloud properties over ocean and its implication for aerosol - cloud
interactions, *J. Geophys. Res.: Atmos.*, 125, e2019JD031598,
730 <https://doi.org/10.1029/2019JD031598>, 2020.
- Blanchard - Wigglesworth, E., Bilbao, R., Donohoe, A., and Materia, S.: Record
warmth of 2023 and 2024 was highly predictable and resulted from ENSO
transition and Northern Hemisphere absorbed shortwave anomalies, *Geophys. Res.*
Lett., 52, e2025GL115614, <https://doi.org/10.1029/2025GL115614>, 2025.
- 735 Boeke, R. C. and Taylor, P. C.: Seasonal energy exchange in sea ice retreat regions
contributes to differences in projected Arctic warming, *Nat. Commun.*, 9, 5017,
<https://doi.org/10.1038/s41467-018-07061-9>, 2018.
- Bony, S., Colman, R., Kattsov, V. M., Allan, R. P., Bretherton, C. S., Dufresne, J.-L.,
Hall, A., Hallegatte, S., Holland, M. M., and Ingram, W.: How well do we
740 understand and evaluate climate change feedback processes?, *J. Clim.*, 19, 3445-
3482, <https://doi.org/10.1175/JCLI3819.1>, 2006.
- Buchard, V., Randles, C., Da Silva, A., Darmenov, A., Colarco, P., Govindaraju, R.,
Ferrare, R., Hair, J., Beyersdorf, A., and Ziemba, L.: The MERRA-2 aerosol
reanalysis, 1980 onward. Part II: Evaluation and case studies, *J. Clim.*, 30, 6851-
745 6872, <https://doi.org/10.1175/JCLI-D-16-0613.1>, 2017.
- Cao, Y., Zhu, Y., Wang, M., Rosenfeld, D., Liang, Y., Liu, J., Liu, Z., and Bai, H.:
Emission reductions significantly reduce the hemispheric contrast in cloud droplet
number concentration in recent two decades, *J. Geophys. Res.: Atmos.*, 128,
e2022JD037417, <https://doi.org/10.1029/2022JD037417>, 2023.
- 750 Ceppi, P. and Hartmann, D. L.: Clouds and the atmospheric circulation response to



- warming, *J. Clim.*, 29, 783-799, <https://doi.org/10.1175/JCLI-D-15-0394.1>, 2016.
- Chen, C., Park, T., Wang, X., Piao, S., Xu, B., Chaturvedi, R. K., Fuchs, R., Brovkin, V., Ciais, P., and Fensholt, R.: China and India lead in greening of the world through land-use management, *Nat. Sustainability*, 2, 122-129, <https://doi.org/10.1038/s41893-019-0220-7>, 2019.
- 755
- Cheng, L., Abraham, J., Trenberth, K. E., Reagan, J., Zhang, H.-M., Storto, A., Von Schuckmann, K., Pan, Y., Zhu, Y., and Mann, M. E.: Record high temperatures in the ocean in 2024, *Adv. Atmos. Sci.*, 42, 1092-1109, <https://doi.org/10.1007/s00376-025-4541-3>, 2025.
- 760
- Colman, R.: Climate radiative feedbacks and adjustments at the Earth's surface, *J. Geophys. Res.: Atmos.*, 120, 3173-3182, <https://doi.org/10.1002/2014JD022896>, 2015.
- Diamond, M. S., Gristey, J. J., Feingold, G., and CSD, E.: Testing Cloud Adjustment Hypotheses for the Maintenance of Earth's Hemispheric Albedo Symmetry with
- 765
- Observed Trends and Natural Experiments, *Geophys. Res. Lett.*, 51, e2024GL111733, <https://doi.org/10.1029/2024GL111733>, 2024.
- Ding, J., Chen, J., and Tang, W.: Increasing trend of precipitable water vapor in Antarctica and Greenland, *China Satellite Navigation Conference*, 286-296, https://doi.org/10.1007/978-981-19-2588-7_27,
- 770
- Dong, T., Zeng, Z., Pan, M., Wang, D., Chen, Y., Liang, L., Yang, S., Jin, Y., Luo, S., and Liang, S.: Record-breaking 2023 marine heatwaves, *Science*, 389, 369-374, <https://doi.org/10.1126/science.adr0910>, 2025.
- Donohoe, A. and Battisti, D. S.: Atmospheric and surface contributions to planetary albedo, *J. Clim.*, 24, 4402-4418, <https://doi.org/10.1175/2011JCLI3946.1>, 2011.
- 775
- Donohoe, A. and Battisti, D. S.: The seasonal cycle of atmospheric heating and temperature, *J. Clim.*, 26, 4962-4980, <https://doi.org/10.1175/JCLI-D-12-00713.1>, 2013.
- Georgakakos, K. P. and Bras, R. L.: A hydrologically useful station precipitation model:
1. Formulation, *Water Resour. Res.*, 20, 1585-1596,
- 780
- <https://doi.org/10.1029/WR020i011p01585>, 1984.
- Global Modeling and Assimilation Office (GMAO): MERRA-2 tavgM_2d_aer_Nx: 2d, Monthly mean, Time-averaged, Single-Level, Assimilation, Aerosol Diagnostics V5.12.4 [dataset]. Greenbelt, MD, USA, Goddard Earth Sciences Data and



- Information Services Center (GES DISC).
785 <https://doi.org/10.5067/FH9A0MLJPC7N>, 2015.
- Goessling, H. F., Rackow, T., and Jung, T.: Recent global temperature surge intensified by record-low planetary albedo, *Science*, eadq7280, <https://doi.org/10.1126/science.adq7280>, 2024.
- Gould, C. F., Heft-Neal, S., Heaney, A. K., Bendavid, E., Callahan, C. W., Kiang, M.
790 V., Graff Zivin, J., and Burke, M.: Temperature extremes impact mortality and morbidity differently, *Sci. Adv.*, 11, eadr3070, <https://doi.org/10.1126/sciadv.adr3070>, 2025.
- Grise, K. M. and Medeiros, B.: Understanding the varied influence of midlatitude jet position on clouds and cloud radiative effects in observations and global climate
795 models, *J. Clim.*, 29, 9005-9025, <https://doi.org/10.1175/JCLI-D-16-0295.1>, 2016.
- Hadas, O., Datsseris, G., Blanco, J., Bony, S., Caballero, R., Stevens, B., and Kaspi, Y.: The role of baroclinic activity in controlling Earth's albedo in the present and future climates, *Proceedings of the National Academy of Sciences*, 120, e2208778120, <https://doi.org/10.1073/pnas.2208778120>, 2023.
- 800 Hartmann, D. L. and Doelling, D.: On the net radiative effectiveness of clouds, *J. Geophys. Res.: Atmos.*, 96, 869-891, <https://doi.org/10.1029/90JD02065>, 1991.
- Hartmann, D. L., Ockert-Bell, M. E., and Michelsen, M. L.: The effect of cloud type on Earth's energy balance: Global analysis, *J. Clim.*, 1281-1304, [https://doi.org/10.1175/1520-0442\(1992\)005%3C1281:TEOCTO%3E2.0.CO;2](https://doi.org/10.1175/1520-0442(1992)005%3C1281:TEOCTO%3E2.0.CO;2),
805 1992.
- He, M., Hu, Y., Chen, N., Wang, D., Huang, J., and Stamnes, K.: High cloud coverage over melted areas dominates the impact of clouds on the albedo feedback in the Arctic, *Sci. Rep.*, 9, 9529, <https://doi.org/10.1038/s41598-019-44155-w>, 2019.
- Hersbach, H., Bell, B., Berrisford, P., Biavati, G., Horányi, A., Muñoz Sabater, J.,
810 Nicolas, J., Peubey, C., Radu, R., and Rozum, I.: ERA5 monthly averaged data on pressure levels from 1940 to present [dataset], Copernicus Climate Change Service (C3S) Climate Data Store (CDS), 10, <https://doi.org/10.24381/cds.6860a573>, 2023a.
- Hersbach, H., Bell, B., Berrisford, P., Biavati, G., Horányi, A., Muñoz Sabater, J.,
815 Nicolas, J., Peubey, C., Radu, R., Rozum, I., Schepers, D., Simmons, A., Soci, C., Dee, D., and Thépaut, J.-N.: ERA5 monthly averaged data on single levels from



- 1940 to present [dataset], Copernicus Climate Change Service (C3S) Climate Data Store (CDS), 10, 252-266, <https://doi.org/10.24381/cds.f17050d7>, 2023b.
- Hodnebrog, Ø., Myhre, G., Jouan, C., Andrews, T., Forster, P. M., Jia, H., Loeb, N. G.,
820 Olivié, D. J., Paynter, D., and Quaas, J.: Recent reductions in aerosol emissions have increased Earth's energy imbalance, *Commun. Earth Environ.*, 5, 166, <https://doi.org/10.1038/s43247-024-01324-8>, 2024.
- Izumi, K., Bartlein, P. J., and Harrison, S. P.: Energy-balance mechanisms underlying consistent large-scale temperature responses in warm and cold climates, *Clim. Dyn.*, 44, 3111-3127, <https://doi.org/10.1007/s00382-014-2189-2>, 2015.
- Jian, B., Li, J., Wang, G., He, Y., Han, Y., Zhang, M., and Huang, J.: The Impacts of Atmospheric and Surface Parameters on Long-Term Variations in the Planetary Albedo, *J. Clim.*, 31, 8705-8718, <https://doi.org/10.1175/jcli-d-17-0848.1>, 2018.
- Kato, S., Rose, F. G., Rutan, D. A., Thorsen, T. J., Loeb, N. G., Doelling, D. R., Huang,
830 X., Smith, W. L., Su, W., and Ham, S.-H.: Surface irradiances of edition 4.0 clouds and the earth's radiant energy system (CERES) energy balanced and filled (EBAF) data product, *J. Clim.*, 31, 4501-4527, <https://doi.org/10.1175/JCLI-D-17-0523.1>, 2018.
- Kaufman, Y. J., Koren, I., Remer, L. A., Rosenfeld, D., and Rudich, Y.: The effect of
835 smoke, dust, and pollution aerosol on shallow cloud development over the Atlantic Ocean, *Proceedings of the National Academy of Sciences*, 102, 11207-11212, <https://doi.org/10.1073/pnas.0505191102>, 2005.
- Kim, B.-M., Hong, J.-Y., Jun, S.-Y., Zhang, X., Kwon, H., Kim, S.-J., Kim, J.-H., Kim, S.-W., and Kim, H.-K.: Major cause of unprecedented Arctic warming in January
840 2016: Critical role of an Atlantic windstorm, *Sci. Rep.*, 7, 40051, <https://doi.org/10.1038/srep40051>, 2017.
- King, M. D., Kaufman, Y. J., Menzel, W. P., and Tanre, D.: Remote sensing of cloud, aerosol, and water vapor properties from the moderate resolution imaging spectrometer(MODIS), *IEEE Trans. Geosci. Remote Sens.*, 30, 2-27,
845 <https://doi.org/10.1109/36.124212>, 1992.
- Klein, S. A., Hall, A., Norris, J. R., and Pincus, R.: Low-cloud feedbacks from cloud-controlling factors: A review, *Shallow clouds, water vapor, circulation, and climate sensitivity*, 38, 1307–1329, <https://doi.org/10.1007/s10712-017-9433-3>, 2017.
- Lapere, R., Thomas, J. L., Marelle, L., Ekman, A. M., Frey, M. M., Lund, M. T.,



- 850 Makkonen, R., Ranjithkumar, A., Salter, M. E., and Samset, B. H.: The representation of sea salt aerosols and their role in polar climate within CMIP6, *J. Geophys. Res.: Atmos.*, 128, e2022JD038235, <https://doi.org/10.1029/2022JD038235>, 2023.
- Lapere, R., Thomas, J. L., Marelle, L., Ekman, A. M., Frey, M. M., Lund, M. T.,
855 Makkonen, R., Ranjithkumar, A., Salter, M. E., and Samset, B. H.: The representation of sea salt aerosols and their role in polar climate within CMIP6, *J. Geophys. Res.: Atmos.*, 128, e2022JD038235, <https://doi.org/10.1029/2022JD038235>, 2023.
- Lelli, L., Vountas, M., Khosravi, N., and Burrows, J. P.: Satellite remote sensing of
860 regional and seasonal Arctic cooling showing a multi-decadal trend towards brighter and more liquid clouds, *Atmos. Chem. Phys.*, 23, 2579-2611, <https://doi.org/10.5194/acp-23-2579-2023>, 2023.
- Li, J., Wang, Y., Li, J., Zhang, W., Zhang, L., and Wang, Y.: Strong aerosol indirect radiative effect from dynamic-driven diurnal variations of cloud water adjustments,
865 *Atmos. Chem. Phys.*, 25, 17455-17472, <https://doi.org/10.5194/acp-25-17455-2025>, 2025a.
- Li, J., Jian, B., Huang, J., Hu, Y., Zhao, C., Kawamoto, K., Liao, S., and Wu, M.: Long-term variation of cloud droplet number concentrations from space-based Lidar, *Remote Sens. Environ.*, 213, 144-161, <https://doi.org/10.1016/j.rse.2018.05.011>,
870 2018.
- Li, K., Zheng, F., Zhu, J., and Zeng, Q.-C.: El Niño and the AMO sparked the astonishingly large margin of warming in the global mean surface temperature in 2023, <https://doi.org/10.1007/s00376-023-3371-4>, 2024a.
- Li, R., Jian, B., Li, J., Wen, D., Zhang, L., Wang, Y., and Wang, Y.: Understanding the
875 trends in reflected solar radiation: a latitude-and month-based perspective, *Atmos. Chem. Phys.*, 24, 9777-9803, <http://dx.doi.org/10.5194/acp-24-9777-2024>, 2024b.
- Li, R., Jian, B., Li, J., Li, J., Cao, Z., Wang, Y., Wang, Y., and Huang, J.: Planetary albedo and reflected shortwave flux: Basic characteristics, mechanisms of change and future projections, *Earth Sci. Rev.*, 105274,
880 <https://doi.org/10.1016/j.earscirev.2025.105274>, 2025b.
- Li, Y., Ge, J., Hu, Y., Xu, Z., Du, J., and Mu, Q.: Global Low Clouds Evolution and Their Meteorological Drivers Across Multiple Timescales, *Remote Sens.*, 17, 4045,



<https://doi.org/10.3390/rs17244045>, 2025c.

Liu, L., Huang, Y., and Gyakum, J. R.: Clouds reduce downwelling longwave radiation
885 over land in a warming climate, *Nature*, 637, 868-874,
<https://doi.org/10.1038/s41586-024-08323-x>, 2025.

Liu, Y., Huang, Y., Yuan, J., Xie, Y., and Zhou, C.: Contribution of surface radiative
effects, heat fluxes and their interactions to land surface temperature variability, *J.*
Geophys. Res.: Atmos., 129, e2023JD039495,
890 <https://doi.org/10.1029/2023JD039495>, 2024.

Loeb, N. G., Johnson, G. C., Thorsen, T. J., Lyman, J. M., Rose, F. G., and Kato, S.:
Satellite and ocean data reveal marked increase in Earth's heating rate, *Geophys.*
Res. Lett., 48, e2021GL093047, <https://doi.org/10.1029/2021GL093047>, 2021.

Loeb, N. G., Thorsen, T. J., Kato, S., Rose, F. G., Hodnebrog, Ø., and Myhre, G.:
895 Emerging hemispheric asymmetry of Earth's radiation, *Proceedings of the*
National Academy of Sciences, 122, e2511595122,
<https://doi.org/10.1073/pnas.2511595122>, 2025.

Loeb, N. G., Ham, S.-H., Allan, R. P., Thorsen, T. J., Meyssignac, B., Kato, S., Johnson,
G. C., and Lyman, J. M.: Observational Assessment of Changes in Earth's Energy
900 Imbalance Since 2000, *Surv. Geophys.*, 1-27, <https://doi.org/10.1007/s10712-024-09838-8>, 2024.

Loeb, N. G., Wielicki, B. A., Doelling, D. R., Smith, G. L., Keyes, D. F., Kato, S.,
Manalo-Smith, N., and Wong, T.: Toward optimal closure of the Earth's top-of-
atmosphere radiation budget, *J. Clim.*, 22, 748-766,
905 <https://doi.org/10.1175/2008JCLI2637.1>, 2009.

Loeb, N. G., Doelling, D. R., Wang, H., Su, W., Nguyen, C., Corbett, J. G., Liang, L.,
Mitrescu, C., Rose, F. G., and Kato, S.: Clouds and the earth's radiant energy
system (CERES) energy balanced and filled (EBAF) top-of-atmosphere (TOA)
edition-4.0 data product, *J. Clim.*, 31, 895-918, <https://doi.org/10.1175/JCLI-D-17-0208.1>, 2018.

Lu, J. and Cai, M.: Seasonality of polar surface warming amplification in climate
simulations, *Geophys. Res. Lett.*, 36, <https://doi.org/10.1029/2009GL040133>,
2009.

Lu, X., Rosenfeld, D., Zhu, Y., Mao, F., Pan, Z., Zang, L., and Gong, W.: Satellite
915 retrievals show adiabatic fraction of marine low clouds decreasing with increasing



- temperature and height above cloud base, *J. Geophys. Res.: Atmos.*, 130, e2024JD043178, <https://doi.org/10.1029/2024JD043178>, 2025.
- 920 Mahesh, A., Gray, M. A., Palm, S. P., Hart, W. D., and Spinhirne, J. D.: Passive and active detection of clouds: Comparisons between MODIS and GLAS observations, *Geophys. Res. Lett.*, 31, <https://doi.org/10.1029/2003GL018859>, 2004.
- Minobe, S., Behrens, E., Findell, K. L., Loeb, N. G., Meyssignac, B., and Sutton, R.: Global and regional drivers for exceptional climate extremes in 2023-2024: beyond the new normal, *npj Clim. Atmos. Sci.*, 8, 138, <https://doi.org/10.1038/s41612-025-00996-z>, 2025.
- 925 Miyamoto, A., Xie, S.-P., and Deser, C.: Unforced interannual to decadal variability of global radiation imbalance: Role of low clouds, *J. Clim.*, e250320, <https://doi.org/10.1175/JCLI-D-25-0320.1>, 2026.
- Myers, T. A., Mechoso, C. R., Cesana, G. V., DeFlorio, M. J., and Waliser, D. E.: Cloud feedback key to marine heatwave off Baja California, *Geophys. Res. Lett.*, 45, 4345-4352, <http://dx.doi.org/10.1029/2018GL078242>, 2018.
- 930 NASA/LARC/SD/ASDC: CERES Monthly Daytime Mean Regionally Averaged Terra and Aqua TOA Fluxes and Associated Cloud Properties Stratified by Optical Depth and Effective Pressure Edition4A [Dataset]. NASA Langley Atmospheric Science Data Center DAAC. Retrieved from https://doi.org/10.5067/Terra-Aqua/CERES/FLUXBYCLDTYP-MONTH_L3.004A, 2020
- 935 NASA/LARC/SD/ASDC: CERES Energy Balanced and Filled (EBAF) TOA and Surface Monthly means data in netCDF Edition 4.2.1 [Dataset]. NASA Langley Atmospheric Science Data Center DAAC. Retrieved from https://doi.org/10.5067/TERRA-AQUA-NOAA20/CERES/EBAF_L3B004.2.1, 2025
- 940 Naud, C. M., Elsaesser, G. S., and Booth, J. F.: Dominant cloud controlling factors for low-level cloud fraction: Subtropical versus extratropical oceans, *Geophys. Res. Lett.*, 50, e2023GL104496, <https://doi.org/10.1029/2023GL104496>, 2023.
- Naud, C. M., Elsaesser, G. S., and Booth, J. F.: A map of dominant cloud-controlling factors for cloud fraction and total liquid water path can identify marine low-level cloud types, *J. Geophys. Res.: Atmos.*, 130, e2025JD044503, <https://doi.org/10.1029/2025JD044503>, 2025.
- 945 Patel, V. K. and Kuttippurath, J.: Increase in tropospheric water vapor amplifies global



- warming and climate change, *Ocean-Land-Atmosphere Research*, 2, 0015,
950 <https://doi.org/10.34133/olar.0015>, 2023.
- Qu, X., Hall, A., Klein, S. A., and Caldwell, P. M.: The strength of the tropical inversion
and its response to climate change in 18 CMIP5 models, *Clim. Dyn.*, 45, 375-396,
<https://doi.org/10.1007/s00382-014-2441-9>, 2015.
- Randles, C., Da Silva, A., Buchard, V., Colarco, P., Darmenov, A., Govindaraju, R.,
955 Smirnov, A., Holben, B., Ferrare, R., and Hair, J.: The MERRA-2 aerosol
reanalysis, 1980 onward. Part I: System description and data assimilation
evaluation, *J. Clim.*, 30, 6823-6850, [10.1175/JCLI-D-16-0609.1](https://doi.org/10.1175/JCLI-D-16-0609.1), 2017.
- Reichler, T., Dameris, M., and Sausen, R.: Determining the tropopause height from
gridded data, *Geophys. Res. Lett.*, 30, <https://doi.org/10.1029/2003GL018240>,
960 2003.
- Ripple, W. J., Wolf, C., Gregg, J. W., Rockström, J., Mann, M. E., Oreskes, N., Lenton,
T. M., Rahmstorf, S., Newsome, T. M., and Xu, C.: The 2024 state of the climate
report: Perilous times on planet Earth, *Bioscience*, 74, 812-824,
<https://doi.org/10.1093/biosci/biae087>, 2024.
- 965 Alkama, R., Taylor, P. C., Garcia-San Martin, L., Douville, H., Duveiller, G., Forzieri,
G., Swingedouw, D., and Cescatti, A.: Clouds damp the radiative impacts of polar
sea ice loss, *The Cryosphere*, 14, 2673-2686, [https://doi.org/10.5194/tc-14-2673-](https://doi.org/10.5194/tc-14-2673-2020)
2020, 2020.
- Andersen, H., Cermak, J., Zipfel, L., and Myers, T. A.: Attribution of observed recent
970 decrease in low clouds over the Northeastern Pacific to cloud-controlling factors,
Geophys. Res. Lett., 49, e2021GL096498,
<https://doi.org/10.1029/2021GL096498>, 2022.
- Andrews, T., Forster, P. M., and Gregory, J. M.: A surface energy perspective on climate
change, *J. Clim.*, 22, 2557-2570, <https://doi.org/10.1175/2008JCLI2759.1>, 2009.
- 975 Arking, A.: The radiative effects of clouds and their impact on climate, *Bull. Am.
Meteorol. Soc.*, 72, 795-814, [https://doi.org/10.1175/1520-](https://doi.org/10.1175/1520-0477(1991)072%3C0795:TREOCA%3E2.0.CO;2)
0477(1991)072%3C0795:TREOCA%3E2.0.CO;2, 1991.
- Bai, H., Wang, M., Zhang, Z., and Liu, Y.: Synergetic satellite trend analysis of aerosol
and warm cloud properties ver ocean and its implication for aerosol - cloud
980 interactions, *J. Geophys. Res.: Atmos.*, 125, e2019JD031598,
<https://doi.org/10.1029/2019JD031598>, 2020.



- Blanchard - Wrigglesworth, E., Bilbao, R., Donohoe, A., and Materia, S.: Record warmth of 2023 and 2024 was highly predictable and resulted from ENSO transition and Northern Hemisphere absorbed shortwave anomalies, *Geophys. Res. Lett.*, 52, e2025GL115614, <https://doi.org/10.1029/2025GL115614>, 2025.
- 985
- Boeke, R. C. and Taylor, P. C.: Seasonal energy exchange in sea ice retreat regions contributes to differences in projected Arctic warming, *Nat. Commun.*, 9, 5017, <https://doi.org/10.1038/s41467-018-07061-9>, 2018.
- Bony, S., Colman, R., Kattsov, V. M., Allan, R. P., Bretherton, C. S., Dufresne, J.-L., Hall, A., Hallegatte, S., Holland, M. M., and Ingram, W.: How well do we understand and evaluate climate change feedback processes?, *J. Clim.*, 19, 3445-3482, <https://doi.org/10.1175/JCLI3819.1>, 2006.
- 990
- Buchard, V., Randles, C., Da Silva, A., Darmenov, A., Colarco, P., Govindaraju, R., Ferrare, R., Hair, J., Beyersdorf, A., and Ziemba, L.: The MERRA-2 aerosol reanalysis, 1980 onward. Part II: Evaluation and case studies, *J. Clim.*, 30, 6851-6872, <https://doi.org/10.1175/JCLI-D-16-0613.1>, 2017.
- 995
- Cao, Y., Zhu, Y., Wang, M., Rosenfeld, D., Liang, Y., Liu, J., Liu, Z., and Bai, H.: Emission reductions significantly reduce the hemispheric contrast in cloud droplet number concentration in recent two decades, *J. Geophys. Res.: Atmos.*, 128, e2022JD037417, <https://doi.org/10.1029/2022JD037417>, 2023.
- 1000
- Ceppi, P. and Hartmann, D. L.: Clouds and the atmospheric circulation response to warming, *J. Clim.*, 29, 783-799, <https://doi.org/10.1175/JCLI-D-15-0394.1>, 2016.
- Chen, C., Park, T., Wang, X., Piao, S., Xu, B., Chaturvedi, R. K., Fuchs, R., Brovkin, V., Ciais, P., and Fensholt, R.: China and India lead in greening of the world through land-use management, *Nat. Sustainability*, 2, 122-129, <https://doi.org/10.1038/s41893-019-0220-7>, 2019.
- 1005
- Cheng, L., Abraham, J., Trenberth, K. E., Reagan, J., Zhang, H.-M., Storto, A., Von Schuckmann, K., Pan, Y., Zhu, Y., and Mann, M. E.: Record high temperatures in the ocean in 2024, *Adv. Atmos. Sci.*, 42, 1092-1109, <https://doi.org/10.1007/s00376-025-4541-3>, 2025.
- 1010
- Colman, R.: Climate radiative feedbacks and adjustments at the Earth's surface, *J. Geophys. Res.: Atmos.*, 120, 3173-3182, <https://doi.org/10.1002/2014JD022896>, 2015.
- Diamond, M. S., Gristey, J. J., Feingold, G., and CSD, E.: Testing Cloud Adjustment



- 1015 Hypotheses for the Maintenance of Earth's Hemispheric Albedo Symmetry with
Observed Trends and Natural Experiments, *Geophys. Res. Lett.*, 51,
e2024GL111733, <https://doi.org/10.1029/2024GL111733>, 2024.
- Ding, J., Chen, J., and Tang, W.: Increasing trend of precipitable water vapor in
Antarctica and Greenland, *China Satellite Navigation Conference*, 286-296,
1020 https://doi.org/10.1007/978-981-19-2588-7_27,
- Dong, T., Zeng, Z., Pan, M., Wang, D., Chen, Y., Liang, L., Yang, S., Jin, Y., Luo, S.,
and Liang, S.: Record-breaking 2023 marine heatwaves, *Science*, 389, 369-374,
<https://doi.org/10.1126/science.adr0910>, 2025.
- Donohoe, A. and Battisti, D. S.: Atmospheric and surface contributions to planetary
1025 albedo, *J. Clim.*, 24, 4402-4418, <https://doi.org/10.1175/2011JCLI3946.1>, 2011.
- Donohoe, A. and Battisti, D. S.: The seasonal cycle of atmospheric heating and
temperature, *J. Clim.*, 26, 4962-4980, <https://doi.org/10.1175/JCLI-D-12-00713.1>,
2013.
- Georgakakos, K. P. and Bras, R. L.: A hydrologically useful station precipitation model:
1030 1. Formulation, *Water Resour. Res.*, 20, 1585-1596,
<https://doi.org/10.1029/WR020i011p01585>, 1984.
- Goessling, H. F., Rackow, T., and Jung, T.: Recent global temperature surge intensified
by record-low planetary albedo, *Science*, eadq7280,
<https://doi.org/10.1126/science.adq7280>, 2024.
- 1035 Gould, C. F., Heft-Neal, S., Heaney, A. K., Bendavid, E., Callahan, C. W., Kiang, M.
V., Graff Zivin, J., and Burke, M.: Temperature extremes impact mortality and
morbidity differently, *Sci. Adv.*, 11, eadr3070,
<https://doi.org/10.1126/sciadv.adr3070>, 2025.
- Grise, K. M. and Medeiros, B.: Understanding the varied influence of midlatitude jet
1040 position on clouds and cloud radiative effects in observations and global climate
models, *J. Clim.*, 29, 9005-9025, <https://doi.org/10.1175/JCLI-D-16-0295.1>, 2016.
- Hadas, O., Datsiris, G., Blanco, J., Bony, S., Caballero, R., Stevens, B., and Kaspi, Y.:
The role of baroclinic activity in controlling Earth's albedo in the present and
future climates, *Proceedings of the National Academy of Sciences*, 120,
1045 e2208778120, <https://doi.org/10.1073/pnas.2208778120>, 2023.
- Hartmann, D. L. and Doelling, D.: On the net radiative effectiveness of clouds, *J.
Geophys. Res.: Atmos.*, 96, 869-891, <https://doi.org/10.1029/90JD02065>, 1991.



- Hartmann, D. L., Ockert-Bell, M. E., and Michelsen, M. L.: The effect of cloud type on Earth's energy balance: Global analysis, *J. Clim.*, 1281-1304, 1050 [https://doi.org/10.1175/1520-0442\(1992\)005%3C1281:TEOCTO%3E2.0.CO;2](https://doi.org/10.1175/1520-0442(1992)005%3C1281:TEOCTO%3E2.0.CO;2), 1992.
- He, M., Hu, Y., Chen, N., Wang, D., Huang, J., and Stamnes, K.: High cloud coverage over melted areas dominates the impact of clouds on the albedo feedback in the Arctic, *Sci. Rep.*, 9, 9529, <https://doi.org/10.1038/s41598-019-44155-w>, 2019.
- 1055 Hersbach, H., Bell, B., Berrisford, P., Biavati, G., Horányi, A., Muñoz Sabater, J., Nicolas, J., Peubey, C., Radu, R., and Rozum, I.: ERA5 monthly averaged data on pressure levels from 1940 to present, Copernicus Climate Change Service (C3S) Climate Data Store (CDS), 10, <https://doi.org/10.24381/cds.6860a573>, 2023a.
- Hersbach, H., Bell, B., Berrisford, P., Biavati, G., Horányi, A., Muñoz Sabater, J., 1060 Nicolas, J., Peubey, C., Radu, R., Rozum, I., Schepers, D., Simmons, A., Soci, C., Dee, D., and Thépaut, J.-N.: ERA5 monthly averaged data on single levels from 1940 to present, Copernicus Climate Change Service (C3S) Climate Data Store (CDS), 10, 252-266, <https://doi.org/10.24381/cds.f17050d7>, 2023b.
- Hodnebrog, Ø., Myhre, G., Jouan, C., Andrews, T., Forster, P. M., Jia, H., Loeb, N. G., 1065 Olivié, D. J., Paynter, D., and Quaas, J.: Recent reductions in aerosol emissions have increased Earth's energy imbalance, *Commun. Earth Environ.*, 5, 166, <https://doi.org/10.1038/s43247-024-01324-8>, 2024.
- Izumi, K., Bartlein, P. J., and Harrison, S. P.: Energy-balance mechanisms underlying consistent large-scale temperature responses in warm and cold climates, *Clim. Dyn.*, 44, 3111-3127, <https://doi.org/10.1007/s00382-014-2189-2>, 2015.
- 1070 Jian, B., Li, J., Wang, G., He, Y., Han, Y., Zhang, M., and Huang, J.: The Impacts of Atmospheric and Surface Parameters on Long-Term Variations in the Planetary Albedo, *J. Clim.*, 31, 8705-8718, <https://doi.org/10.1175/jcli-d-17-0848.1>, 2018.
- Kato, S., Rose, F. G., Rutan, D. A., Thorsen, T. J., Loeb, N. G., Doelling, D. R., Huang, 1075 X., Smith, W. L., Su, W., and Ham, S.-H.: Surface irradiances of edition 4.0 clouds and the earth's radiant energy system (CERES) energy balanced and filled (EBAF) data product, *J. Clim.*, 31, 4501-4527, <https://doi.org/10.1175/JCLI-D-17-0523.1>, 2018.
- Kaufman, Y. J., Koren, I., Remer, L. A., Rosenfeld, D., and Rudich, Y.: The effect of 1080 smoke, dust, and pollution aerosol on shallow cloud development over the Atlantic



- Ocean, *Proceedings of the National Academy of Sciences*, 102, 11207-11212, <https://doi.org/10.1073/pnas.0505191102>, 2005.
- Kim, B.-M., Hong, J.-Y., Jun, S.-Y., Zhang, X., Kwon, H., Kim, S.-J., Kim, J.-H., Kim, S.-W., and Kim, H.-K.: Major cause of unprecedented Arctic warming in January 2016: Critical role of an Atlantic windstorm, *Sci. Rep.*, 7, 40051, <https://doi.org/10.1038/srep40051>, 2017.
- 1085
- King, M. D., Kaufman, Y. J., Menzel, W. P., and Tanre, D.: Remote sensing of cloud, aerosol, and water vapor properties from the moderate resolution imaging spectrometer(MODIS), *IEEE Trans. Geosci. Remote Sens.*, 30, 2-27, <https://doi.org/10.1109/36.124212>, 1992.
- 1090
- Klein, S. A., Hall, A., Norris, J. R., and Pincus, R.: Low-cloud feedbacks from cloud-controlling factors: A review, *Shallow clouds, water vapor, circulation, and climate sensitivity*, 38, 1307–1329, <https://doi.org/10.1007/s10712-017-9433-3>, 2017.
- Lapere, R., Thomas, J. L., Marelle, L., Ekman, A. M., Frey, M. M., Lund, M. T., Makkonen, R., Ranjithkumar, A., Salter, M. E., and Samset, B. H.: The representation of sea salt aerosols and their role in polar climate within CMIP6, *J. Geophys. Res.: Atmos.*, 128, e2022JD038235, <https://doi.org/10.1029/2022JD038235>, 2023.
- 1095
- Lelli, L., Vountas, M., Khosravi, N., and Burrows, J. P.: Satellite remote sensing of regional and seasonal Arctic cooling showing a multi-decadal trend towards brighter and more liquid clouds, *Atmos. Chem. Phys.*, 23, 2579-2611, <https://doi.org/10.5194/acp-23-2579-2023>, 2023.
- 1100
- Li, J., Wang, Y., Li, J., Zhang, W., Zhang, L., and Wang, Y.: Strong aerosol indirect radiative effect from dynamic-driven diurnal variations of cloud water adjustments, *Atmos. Chem. Phys.*, 25, 17455-17472, <https://doi.org/10.5194/acp-25-17455-2025>, 2025a.
- 1105
- Li, J., Jian, B., Huang, J., Hu, Y., Zhao, C., Kawamoto, K., Liao, S., and Wu, M.: Long-term variation of cloud droplet number concentrations from space-based Lidar, *Remote Sens. Environ.*, 213, 144-161, <https://doi.org/10.1016/j.rse.2018.05.011>, 2018.
- 1110
- Li, K., Zheng, F., Zhu, J., and Zeng, Q.-C.: El Niño and the AMO sparked the astonishingly large margin of warming in the global mean surface temperature in 2023, <https://doi.org/10.1007/s00376-023-3371-4>, 2024a.



- 1115 Li, R., Jian, B., Li, J., Wen, D., Zhang, L., Wang, Y., and Wang, Y.: Understanding the trends in reflected solar radiation: a latitude-and month-based perspective, *Atmos. Chem. Phys.*, 24, 9777-9803, <http://dx.doi.org/10.5194/acp-24-9777-2024>, 2024b.
- Li, R., Jian, B., Li, J., Li, J., Cao, Z., Wang, Y., Wang, Y., and Huang, J.: Planetary albedo and reflected shortwave flux: Basic characteristics, mechanisms of change and future projections, *Earth Sci. Rev.*, 105274, <https://doi.org/10.1016/j.earscirev.2025.105274>, 2025b.
- 1120 Li, Y., Ge, J., Hu, Y., Xu, Z., Du, J., and Mu, Q.: Global Low Clouds Evolution and Their Meteorological Drivers Across Multiple Timescales, *Remote Sens.*, 17, 4045, <https://doi.org/10.3390/rs17244045>, 2025c.
- Liu, L., Huang, Y., and Gyakum, J. R.: Clouds reduce downwelling longwave radiation over land in a warming climate, *Nature*, 637, 868-874, <https://doi.org/10.1038/s41586-024-08323-x>, 2025.
- Liu, Y., Huang, Y., Yuan, J., Xie, Y., and Zhou, C.: Contribution of surface radiative effects, heat fluxes and their interactions to land surface temperature variability, *J. Geophys. Res.: Atmos.*, 129, e2023JD039495, <https://doi.org/10.1029/2023JD039495>, 2024.
- 1130 Loeb, N. G., Johnson, G. C., Thorsen, T. J., Lyman, J. M., Rose, F. G., and Kato, S.: Satellite and ocean data reveal marked increase in Earth's heating rate, *Geophys. Res. Lett.*, 48, e2021GL093047, <https://doi.org/10.1029/2021GL093047>, 2021.
- Loeb, N. G., Thorsen, T. J., Kato, S., Rose, F. G., Hodnebrog, Ø., and Myhre, G.: 1135 Emerging hemispheric asymmetry of Earth's radiation, *Proceedings of the National Academy of Sciences*, 122, e2511595122, <https://doi.org/10.1073/pnas.2511595122>, 2025.
- Loeb, N. G., Ham, S.-H., Allan, R. P., Thorsen, T. J., Meyssignac, B., Kato, S., Johnson, G. C., and Lyman, J. M.: Observational Assessment of Changes in Earth's Energy 1140 Imbalance Since 2000, *Surv. Geophys.*, 1-27, <https://doi.org/10.1007/s10712-024-09838-8>, 2024.
- Loeb, N. G., Wielicki, B. A., Doelling, D. R., Smith, G. L., Keyes, D. F., Kato, S., Manalo-Smith, N., and Wong, T.: Toward optimal closure of the Earth's top-of-atmosphere radiation budget, *J. Clim.*, 22, 748-766, <https://doi.org/10.1175/2008JCLI2637.1>, 2009.
- 1145 Loeb, N. G., Doelling, D. R., Wang, H., Su, W., Nguyen, C., Corbett, J. G., Liang, L.,



- Mitrescu, C., Rose, F. G., and Kato, S.: Clouds and the earth's radiant energy system (CERES) energy balanced and filled (EBAF) top-of-atmosphere (TOA) edition-4.0 data product, *J. Clim.*, 31, 895-918, <https://doi.org/10.1175/JCLI-D-17-0208.1>, 2018.
- 1150
- Lu, J. and Cai, M.: Seasonality of polar surface warming amplification in climate simulations, *Geophys. Res. Lett.*, 36, <https://doi.org/10.1029/2009GL040133>, 2009.
- Lu, X., Rosenfeld, D., Zhu, Y., Mao, F., Pan, Z., Zang, L., and Gong, W.: Satellite retrievals show adiabatic fraction of marine low clouds decreasing with increasing temperature and height above cloud base, *J. Geophys. Res.: Atmos.*, 130, e2024JD043178, <https://doi.org/10.1029/2024JD043178>, 2025.
- 1155
- Mahesh, A., Gray, M. A., Palm, S. P., Hart, W. D., and Spinhirne, J. D.: Passive and active detection of clouds: Comparisons between MODIS and GLAS observations, *Geophys. Res. Lett.*, 31, <https://doi.org/10.1029/2003GL018859>, 2004.
- 1160
- Minobe, S., Behrens, E., Findell, K. L., Loeb, N. G., Meyssignac, B., and Sutton, R.: Global and regional drivers for exceptional climate extremes in 2023-2024: beyond the new normal, *npj Clim. Atmos. Sci.*, 8, 138, <https://doi.org/10.1038/s41612-025-00996-z>, 2025.
- 1165
- Miyamoto, A., Xie, S.-P., and Deser, C.: Unforced interannual to decadal variability of global radiation imbalance: Role of low clouds, *J. Clim.*, e250320, <https://doi.org/10.1175/JCLI-D-25-0320.1>, 2026.
- Myers, T. A., Mechoso, C. R., Cesana, G. V., DeFlorio, M. J., and Waliser, D. E.: Cloud feedback key to marine heatwave off Baja California, *Geophys. Res. Lett.*, 45, 4345-4352, <http://dx.doi.org/10.1029/2018GL078242>, 2018.
- 1170
- Naud, C. M., Elsaesser, G. S., and Booth, J. F.: Dominant cloud controlling factors for low-level cloud fraction: Subtropical versus extratropical oceans, *Geophys. Res. Lett.*, 50, e2023GL104496, <https://doi.org/10.1029/2023GL104496>, 2023.
- Naud, C. M., Elsaesser, G. S., and Booth, J. F.: A map of dominant cloud-controlling factors for cloud fraction and total liquid water path can identify marine low-level cloud types, *J. Geophys. Res.: Atmos.*, 130, e2025JD044503, <https://doi.org/10.1029/2025JD044503>, 2025.
- 1175
- Patel, V. K. and Kuttippurath, J.: Increase in tropospheric water vapor amplifies global warming and climate change, *Ocean-Land-Atmosphere Research*, 2, 0015,



- 1180 <https://doi.org/10.34133/olar.0015>, 2023.
- Qu, X., Hall, A., Klein, S. A., and Caldwell, P. M.: The strength of the tropical inversion and its response to climate change in 18 CMIP5 models, *Clim. Dyn.*, 45, 375-396, <https://doi.org/10.1007/s00382-014-2441-9>, 2015.
- Randles, C., Da Silva, A., Buchard, V., Colarco, P., Darmenov, A., Govindaraju, R.,
1185 Smirnov, A., Holben, B., Ferrare, R., and Hair, J.: The MERRA-2 aerosol reanalysis, 1980 onward. Part I: System description and data assimilation evaluation, *J. Clim.*, 30, 6823-6850, [10.1175/JCLI-D-16-0609.1](https://doi.org/10.1175/JCLI-D-16-0609.1), 2017.
- Reichler, T., Dameris, M., and Sausen, R.: Determining the tropopause height from gridded data, *Geophys. Res. Lett.*, 30, <https://doi.org/10.1029/2003GL018240>,
1190 2003.
- Ripple, W. J., Wolf, C., Gregg, J. W., Rockström, J., Mann, M. E., Oreskes, N., Lenton, T. M., Rahmstorf, S., Newsome, T. M., and Xu, C.: The 2024 state of the climate report: Perilous times on planet Earth, *Bioscience*, 74, 812-824, <https://doi.org/10.1093/biosci/biae087>, 2024.
- 1195 Schmale, J., Zieger, P., and Ekman, A. M.: Aerosols in current and future Arctic climate, *Nat. Clim. Change*, 11, 95-105, <https://doi.org/10.1038/s41558-020-00969-5>, 2021.
- Scott, R. C., Myers, T. A., Norris, J. R., Zelinka, M. D., Klein, S. A., Sun, M., and Doelling, D. R.: Observed sensitivity of low-cloud radiative effects to meteorological perturbations over the global oceans, *J. Clim.*, 33, 7717-7734, <https://doi.org/10.1175/JCLI-D-19-1028.1>, 2020.
- 1200 Sejas, S. A., Hu, X., Cai, M., and Fan, H.: Understanding the differences between TOA and surface energy budget attributions of surface warming, *Front. Earth Sci.*, 9, 725816, <https://doi.org/10.3389/feart.2021.725816>, 2021.
- 1205 Stephens, G. L., O'Brien, D., Webster, P. J., Pilewski, P., Kato, S., and Li, J.-l.: The albedo of Earth, *Rev. Geophys.*, 53, 141-163, <https://doi.org/10.1002/2014rg000449>, 2015.
- Sun, M., Doelling, D. R., Loeb, N. G., Scott, R. C., Wilkins, J., Nguyen, L. T., and Mlynczak, P.: Clouds and the Earth's Radiant Energy System (CERES) FluxByCldTyp edition 4 data product, *J. Atmos. Oceanic Technol.*, 39, 303-318, <https://doi.org/10.1175/JTECH-D-21-0029.1>, 2022.
- 1210 Tselioudis, G., Remillard, J., Jakob, C., and Rossow, W. B.: Contraction of the world's



- storm-cloud zones the primary contributor to the 21st century increase in the Earth's sunlight absorption, *Geophys. Res. Lett.*, 52, e2025GL114882, <https://doi.org/10.1029/2025GL114882>, 2025.
- 1215
- Tselioudis, G., Rossow, W. B., Bender, F., Oreopoulos, L., and Remillard, J.: Oceanic cloud trends during the satellite era and their radiative signatures, *Clim. Dyn.*, 62, 9319-9332, <https://doi.org/10.1007/s00382-024-07396-8>, 2024.
- Twohy, C. H., DeMott, P. J., Russell, L. M., Toohey, D. W., Rainwater, B., Geiss, R., Sanchez, K. J., Lewis, S., Roberts, G. C., and Humphries, R. S.: Cloud-nucleating particles over the Southern Ocean in a changing climate, *Earth's Future*, 9, e2020EF001673, <https://doi.org/10.1029/2020EF001673>, 2021.
- 1220
- Viúdez-Mora, A., Costa-Surós, M., Calbó, J., and González, J.: Modeling atmospheric longwave radiation at the surface during overcast skies: The role of cloud base height, *J. Geophys. Res.: Atmos.*, 120, 199-214, <https://doi.org/10.1002/2014JD022310>, 2015.
- 1225
- von Salzen, K., Akingunola, A., Cole, J. N., Digby, R. A., Doherty, S. J., Fraser-Leach, L., Gryspeerdt, E., Sigmond, M., and Wood, R.: Reduced aerosol pollution diminished cloud reflectivity over the North Atlantic and Northeast Pacific, *Nat. Commun.*, 16, 1-10, <https://doi.org/10.1038/s41467-025-65127-x>, 2025.
- 1230
- Wielicki, B. A., Barkstrom, B. R., Harrison, E. F., Lee III, R. B., Smith, G. L., and Cooper, J. E.: Clouds and the Earth's Radiant Energy System (CERES): An earth observing system experiment, *Bull. Am. Meteorol. Soc.*, 77, 853-868, [https://doi.org/10.1175/1520-0477\(1996\)077<0853:CATERE>2.0.CO;2](https://doi.org/10.1175/1520-0477(1996)077<0853:CATERE>2.0.CO;2), 1996.
- 1235
- Wilson Kemsley, S., Ceppi, P., Andersen, H., Cermak, J., Stier, P., and Nowack, P.: A systematic evaluation of high-cloud controlling factors, *Atmos. Chem. Phys.*, 24, 8295-8316, <https://doi.org/10.5194/acp-24-8295-2024>, 2024.
- Wood, R.: Stratocumulus clouds, *Mon. Weather Rev.*, 140, 2373-2423, <https://doi.org/10.1175/MWR-D-11-00121.1>, 2012.
- 1240
- Wood, R. and Bretherton, C. S.: On the relationship between stratiform low cloud cover and lower-tropospheric stability, *J. Clim.*, 19, 6425-6432, <https://doi.org/10.1175/JCLI3988.1>, 2006.
- Woods, C. and Caballero, R.: The role of moist intrusions in winter Arctic warming and sea ice decline, *J. Clim.*, 29, 4473-4485, <https://doi.org/10.1175/JCLI-D-15-0773.1>, 2016.
- 1245



- Wu, D. L., Lee, J. N., Kim, K.-M., and Lim, Y.-K.: Interannual variations of TOA albedo over the Arctic, Antarctic and Tibetan plateau in 2000–2019, *Remote Sens.*, 12, 1460, <https://doi.org/10.3390/rs12091460>, 2020.
- 1250 Wu, M., Zhou, T., Li, C., Li, H., Chen, X., Wu, B., Zhang, W., and Zhang, L.: A very likely weakening of Pacific Walker Circulation in constrained near-future projections, *Nat. Commun.*, 12, 6502, <https://doi.org/10.1038/s41467-021-26693-y>, 2021.
- Yamanouchi, T., Suzuki, K., and Kawaguchi, S.: Detection of clouds in Antarctica from infrared multispectral data of AVHRR, *Journal of the Meteorological Society of Japan*. Ser. II, 65, 949-962, https://doi.org/10.2151/jmsj1965.65.6_949, 1987.
- 1255 Yuan, T., Song, H., Oreopoulos, L., Wood, R., Bian, H., Breen, K., Chin, M., Yu, H., Barahona, D., and Meyer, K.: Abrupt reduction in shipping emission as an inadvertent geoengineering termination shock produces substantial radiative warming, *Commun. Earth Environ.*, 5, 281, <https://doi.org/10.1038/s43247-024-01442-3>, 2024.
- 1260 Zelinka, M. D., Myers, T. A., McCoy, D. T., Po-Chedley, S., Caldwell, P. M., Ceppi, P., Klein, S. A., and Taylor, K. E.: Causes of higher climate sensitivity in CMIP6 models, *Geophys. Res. Lett.*, 47, e2019GL085782, <https://doi.org/10.1029/2019GL085782>, 2020.